R. & M. No. 3230

MINISTRY OF AVIATION

AERONAUTICAL RESEARCH COUNCIL
REPORTS AND MEMORANDA

10-ft x 7-ft Tunnel Tests up to M = 0·94 of Nose Droop and a Blunt-Nosed NACA 3-00 Type Section on a $7\frac{1}{2}$ per cent Thick 50 deg Swept Wing

By A. L. COURTNEY, B.Sc.

LONDON: HER MAJESTY'S STATIONERY OFFICE
1961
FOURTEEN SHILLINGS NET

10-ft x 7-ft Tunnel Tests up to M = 0·94 of Nose Droop and a Blunt-Nosed NACA 3-00 Type Section on a 7½ per cent Thick 50 deg Swept Wing

By A. L. Courtney, B.Sc.

Communicated by the Director-General of Scientific Research (Air), Ministry of Supply

*Reports and Memoranda No. 3230**
March, 1958

Summary. This note describes further tests made during 1954 in the Royal Aircraft Establishment 10 ft × 7 ft High Speed Tunnel, as part of a research programme to improve the subsonic longitudinal stability characteristics of a 50 deg swept wing of aspect ratio 3·1 by means such as nose-droop, chord extensions, fences, change of aerofoil section, etc.

Lift, drag, pitching-moment and root bending moment were measured with the basic 7½ per cent thick RAE 101 section, with a symmetrical blunt-nosed NACA 3–007·5 section, and with a full-span drooped and thickened nose, at Mach numbers up to 0·94 and Reynolds numbers between $1·7 \times 10^6$ and 6×10^6. The main conclusions are as follows:

(i) None of the section changes gives any advantage over the basic RAE 101 section at the highest test Mach numbers.

(ii) The drooped-nose sections are superior to the NACA 3–007·5 section at all Mach numbers.

(iii) The full-span nose-droop is inferior to the part-span droop with the same section tested earlier in the series.

(iv) Better high-speed characteristics should be obtainable by the use of nose-droop without the thickening applied here.

Further conclusions are given in Section 5.

Oil-film flow patterns show several interesting features which are discussed in some detail. Another feature which is discussed is the occurrence of an unusual adverse scale effect on the drooped wings at low Mach number.

1. *Introduction.* Refs. 1 to 3 describe tests in the R.A.E. 10 ft × 7 ft High Speed Wind Tunnel† at Mach numbers up to 0·94 on a 50 deg swept wing with an aspect ratio of 3·1 and a 7½ per cent thick RAE 101 section, with and without stall-fences, part-span leading-edge extensions and part-span leading-edge droop and thickening. One of the objects of these tests was to investigate and improve the pitching-moment behaviour at moderate and high lift coefficients, since on the basic wing the useful C_L range is restricted by loss of stability due to outer-wing flow separation. The various devices gave some increase in the C_L for instability but the improvement was less than hoped for, particularly at the higher subsonic Mach numbers.

* Previously issued as R.A.E. Tech. Note Aero 2,556—A.R.C. 20,332.

† Now the 8 ft × 6 ft Transonic Tunnel.

Following these tests, it was thought[1] that the effectiveness of the leading-edge droop would be greater if it were extended to cover the whole of the span. Droop shape B of Ref. 1 was therefore tested as a full-span modification. Tests were also made on a further full-span droop with increased camber and thickness, referred to as droop C. Finally, to investigate the effects of nose-thickening alone, without camber, a symmetrical NACA 3–007·5 section was tested on the same plan form. The results of these tests are reported here.

In view of the developments that have occurred since the tests were done in 1954, it is perhaps worth noting that the droop shapes investigated were of the kind then being considered for application to swept-wing subsonic fighters, incorporating appreciable thickening near the leading edge. Although this is advantageous at low speeds it would no longer be recommended for high subsonic speeds, where it seems preferable to thin the leading edge rather than thicken it. The present results are thus not of great practical application; they are of interest, however, in relation to the general question of flow behaviour on sweptback wings and are presented and discussed in detail from this standpoint.

Following a description of the models and tests Section 3 deals with the force and flow characteristics at a Mach number of 0·18 and Reynolds numbers of 2×10^6 to 6×10^6, and a summary of the main conclusions from these low-speed tests is given in Section 3.4. Section 4 then discusses the characteristics at Mach numbers up to 0·94 and Reynolds number of $1{\cdot}7 \times 10^6$, and the conclusions are given in Section 5.

2. *Description of Models and Tests.* 2.1. *Wing Planform, etc.* The basic model with the $7\frac{1}{2}$ per cent thick RAE 101 section was that previously tested as wing A in Ref. 2. It had an aspect ratio of 3·1, a quarter-chord sweepback of 50 deg, and a taper ratio of 0·362 disregarding the curved Küchemann tip fairing, *i.e.*, continuing the leading edge straight to the tip. Details are given in Table 1 and Fig. 1.

The model with the NACA 3–007·5 section, which will be referred to as the NACA 3 wing, had the same planform as the basic RAE 101 wing.

The drooped wings, referred to as wings B and C, differed slightly in planform from the others, having leading-edge chord extensions of $0{\cdot}019c$ and $0{\cdot}025c$ respectively, associated with the method adopted for applying the part-span droop in Ref. 1; it was thought desirable to preserve this feature in the tests with full-span droop.

Since at low speeds leading-edge flow separation usually occurs first on the curved tip fairing with which this series of wings was fitted, Ref. 1 suggested that the amount of droop should be increased around the fairing. Because of the high leading-edge sweep in this region it was thought that the nose shape in sections normal to the curved leading-edge might be more important than the chordwise shape; accordingly the additional droop was applied in the spanwise direction leaving the chordwise sections unaltered. The droop was applied by progressively depressing the chord-lines, without twist, between section AA (Fig. 1) and the tip, *i.e.*, applying varying anhedral over the tip fairing. Details are given in Fig. 1.

2.2. *Section Shapes.* Section ordinates for the four wings are given in Table 2. For the drooped wings, B and C, it should be noted that in this table the co-ordinates are given relative to the chordline of the unmodified section. The section shapes are shown in Fig. 2; in the top half the overall shapes are compared with the RAE 101 section, and in the lower half the thickness distributions and the camber-lines are compared separately.

The NACA 3 section is very much thicker near the nose than the RAE 101 section. Its leading-edge radius is $0{\cdot}0119c$ compared with $0{\cdot}0043c$ for RAE 101, and its maximum thickness is at $0{\cdot}185c$ compared with $0{\cdot}31c$. Its nose radius is equal to that of a $12\frac{1}{2}$ per cent thick RAE 101 section. Aft of mid-chord there is little difference between the two sections, RAE 101 tapering slightly more rapidly than NACA 3.

The droop B *nose shape* is the result of gradual development as described in Ref. 1. The shape tested here is that described as droop B_1 in Ref. 1, which differed from the original droop B shape in minor details. The upper-surface shape was obtained by blending into the basic RAE 101 section the nose of a section having the same thickness distribution but with $0{\cdot}015c$ camber on an '$m = 0{\cdot}8$' camber-line[6], so as to fair into the original upper surface as close to the leading-edge as possible without undercutting it (this determined the chord-extension required). The characteristic beak on the lower surface, using this camber-line, was faired over with a large fairing extending aft to about the maximum thickness position. The forward part of this fairing was given the shape of a 10 per cent thick RAE 101 section back to $0{\cdot}065c$ in order to provide a definite and favourable lower-surface profile near the leading-edge, since the poor results obtained with the earlier droop A of Ref. 1 were thought to be due to an unsatisfactory shape in this region.

On breaking down the final droop B ordinates into a mean camber-line and a thickness distribution, as in Fig. 2, it can be seen that the section has a maximum camber of $0{\cdot}013c$ at $0{\cdot}3c$, relative to a chord-line which is twisted $1{\cdot}1$ deg nose-down compared with the basic RAE 101 chord-line. The forward part of the camber-line is roughly similar to the forward part of an '$m = 0{\cdot}4$' camber-line of the same maximum camber. The thickness distribution is appreciably more blunt than that of the RAE 101 section, having a nose radius of $0{\cdot}0106c$ compared with $0{\cdot}0043c$.

The droop C *nose shape* was developed after the tests of Ref. 1 on the part-span droop B modification had been completed. The flow studies on this wing at $R = 2\frac{1}{2} \times 10^6$, $M = 0{\cdot}27$, showed that leading-edge separation still occurred on the outermost drooped sections at high incidence, but on the inner part of the drooped panel there was no separation up to the highest test incidence ($\alpha = 22$ deg). To delay the flow breakdown still further at the tip a more extreme modification was required, and it was decided to take as the basis of design the calculated incompressible pressure distribution near the leading edge at mid-semi-span for droop B, attempting to reproduce this distribution near the tip by using more droop and nose-thickening to counter the tip effect. Droop C was developed to this requirement by successive approximation using the method of Ref. 7 to calculate the pressure distribution.

Droop C has a leading-edge droop of $0{\cdot}0315c$ and a leading-edge extension of $0{\cdot}025c$, compared with $0{\cdot}020c$ and $0{\cdot}019c$ respectively for droop B. It has a very bluff nose (Fig. 2), the nose radius of the thickness distribution being $0{\cdot}0166c$ compared with $0{\cdot}0106c$ for droop B, $0{\cdot}0119c$ for the NACA 3 section and only $0{\cdot}0043c$ for the basic RAE 101 section; it is equivalent to that of a $14{\cdot}7$ per cent thick RAE 101 section. The maximum camber is $0{\cdot}0205c$ at about $0{\cdot}25c$, relative to a chord-line which is twisted $1{\cdot}8$ deg nose-down compared with the basic section chord-line. The forward part of the camber-line is similar in shape to the forward part of an '$m = 0{\cdot}5$' camber-line having the same maximum camber.

2.3. *Description of Tests.* The models were tested using the 'nett half-wing' technique described more fully in Ref. 2. In this method a half-wing was tested using the tunnel floor as a reflection plane, in the presence of a half-body mounted on the floor independently of the wing, so that the

under-floor balance measured only the forces on the exposed nett wing in the presence of the body. The same body was used for all four wings; details are given in Table 1 and Fig. 1.

Since the forces measured were those on the exposed wing, the quoted force coefficients are based on the area and mean chord of the exposed wing, and the pitching-moment axis is at the quarter-chord point of the nett mean chord. The spanwise centre of load, however, is related to the gross semi-span. For wings B and C the wing area and chord are measured to the extended leading edge. The geometrical mean chord is used here, for consistency with earlier tests in the series.

The wings were tested over the Mach number range 0·50 to 0·94 at a Reynolds number of about $1{\cdot}7 \times 10^6$ based on nett mean chord. In addition, tests were made at Reynolds numbers between 2×10^6 and 6×10^6 at a Mach number of 0·18. Upper-surface flow visualization pictures were obtained on each wing at $R \sim 2{\cdot}6 \times 10^6$, $M = 0{\cdot}27$, using the oil-film technique (titanium oxide in light diesel oil) developed at RAE and described in Ref. 2.

The tests were made with free boundary-layer transition in all cases. The RAE 101 wing was tested in 1952 and the results have been fully reported in Ref. 2. The other wings were tested between May and August, 1954.

2.4. *Corrections Applied to the Results.* The observed Mach number and force coefficients have been corrected for model blockage and tunnel wall constraint as described in Ref. 2. The blockage corrections were approximately the same for all four wings; typical values for the RAE 101 wing can be found in Ref. 2.

3. *Results and Discussion*: *Low Mach number* ($M = 0{\cdot}18$). The low-speed results, including flow visualization studies and the effects of Reynolds number, exhibit several interesting features of the flow over sweptback wings, and these will be discussed in some detail before dealing with the higher Mach numbers, at which force results only are available.

Fig. 3 presents curves of C_m against C_L for the four wings at Reynolds numbers of 2×10^6, 4×10^6 and 6×10^6 at $M = 0{\cdot}18$, and Figs. 4, 5 and 6 give curves of C_L against α, $(C_D - C_L^2/\pi A)$ against C_L, and spanwise centre of load against C_L at Reynolds numbers of 2×10^6 and 6×10^6. The results for $R = 4 \times 10^6$ are omitted from Figs. 4 to 6 in the interests of clarity.

The flow over thin swept wings at moderate and high incidence, and the correlation between the flow characteristics and the overall force behaviour, have been discussed in detail in Refs. 1, 2, 3, 5, 8, 9 and elsewhere. In the following discussion some knowledge of the terms and principles involved will be assumed. Also, since the results for the RAE 101 wing have been fully reported in Refs. 1 and 2 they will not be analysed again; they are repeated here for ease of reference since they form the basis of comparison for the other three wings.

3.1. *Comparison of the RAE* 101 *Wing and the Drooped Wings*, B *and* C, *at Low Mach Number.* 3.1.1. *Force characteristics at* $R \sim 2 \times 10^6$. Fig. 3 shows that at $R \sim 2 \times 10^6$ on the basic wing, instability occurs beyond a lift coefficient of about 0·67. On wing B, having the droop B section, severe instability* does not occur until beyond $C_L = 1{\cdot}0$, and on wing C not until beyond $C_L = 1{\cdot}1$, although there is a large reduction in stability near $C_L = 1{\cdot}0$ on this wing. Thus, the drooped and thickened noses of wings B and C have increased the C_L for instability at this Reynolds number by between 0·35 and 0·45 compared with the RAE 101 wing.

* The gradual increase in C_m between $C_L = 0{\cdot}3$ and $C_L = 0{\cdot}7$ is discussed later (Section 3.1.3); it is not of significance in the present context.

On the RAE 101 wing, it is known[1,2] that the loss of stability is due to premature loss of lift curve slope on the outer wing sections, associated with leading-edge laminar separation which is basically of the long-bubble kind. As shown in Fig. 7 droops B and C very greatly reduce the calculated peak value of $(-Cp)$ near the outer-wing leading-edge, from about 20 for the RAE 101 section to only about 4 for droop C at $\alpha = 20$ deg, and calculations suggest that even at the comparatively low Reynolds number of $1{\cdot}8 \times 10^6$ this results in the long-bubble type of separation being suppressed and replaced by a short-bubble type. The advantage of this is that, with the short bubble, no significant loss of section lift slope occurs until the bubble 'bursts', and the lift coefficient at which this happens is appreciably higher than that at which the long bubble on the basic section starts to expand rearward with consequent loss of lift curve slope. As a result, the overall lift coefficients at which given stages of flow development are reached on wings B and C are appreciably greater than those for the basic RAE 101 wing, and this is reflected not only in the increased value of the C_L for loss of stability (above) but also in other respects. For instance, on the basic RAE 101 wing the first appearance of flow separation is marked by a more rapid increase of $(C_D - C_L^2/\pi A)$ with C_L near $C_L = 0{\cdot}4$, as shown in Fig. 5. On wing C this is delayed to near $C_L = 0{\cdot}7$. Also, the beginning of the nose-down trim change, which is due to the effect of the part-span vortex sheet in increasing the lift on the outer sections while it is located near the tip[1], is delayed from $C_L \sim 0{\cdot}4$ on the RAE 101 wing to $C_L \sim 0{\cdot}7$ on wing C. Finally, the increase in the overall lift slope arising from the same cause is similarly delayed (Fig. 4).

It should perhaps be made clear that the term 'long-bubble type of separation', used here in connection with a sweptback wing, is not meant to imply that a typical two-dimensional closed bubble in fact exists on the wing. The mechanism of closure and the detailed structure of the separated region are different for a swept wing. However, the essential characteristic of a long-bubble separation remains, namely the gradual increase of the chordwise extent of the separation with incidence, as distinct from the short-bubble separation which remains of very small chordwise extent having little effect on the pressure distribution until it bursts quite suddenly at a sufficiently high incidence.

3.1.2. *Flow patterns* ($R = 2{\cdot}6 \times 10^6$, $M = 0{\cdot}27$). The changes in the force characteristics between the plain wing and the drooped wings can be roughly* correlated with the changes in the upper-surface oil-film patterns shown in Figs. 8 and 9. Fig. 8 shows the oil-film patterns for the RAE 101 wing at incidences of 8·1 deg, 12·2 deg, 14·2 deg and 16·3 deg (these being the only relevant incidences studied during the early tests of 1952), and Fig. 9 gives the patterns for wing C at incidences between 12·2 deg and 22·3 deg. For the RAE 101 wing some of the pictures are 'final' pictures, taken after most of the oil had been blown off the wing, the fan stopped and the model rotated to be normal to the camera, and some are 'early' pictures taken during the run, before much oil had been blown from the wing. The early pictures show less fine detail, but are useful in showing more clearly the major features of the flow and in particular the position of the part-span vortex sheet, which at any rate on the RAE 101 wing has the effect of rapidly scouring the oil from the wing beneath it, exposing the black wing surface (the oil is white). For wing C the pictures are all of this kind. Different cases should not be compared on the basis of the degree of whiteness of the pictures.

* Close correlation cannot be expected in view of the differences in test conditions—$M = 0{\cdot}18$, $R \sim 2 \times 10^6$ for the force results and $M = 0{\cdot}27$, $R = 2{\cdot}6 \times 10^6$ for the flow pictures.

On the RAE 101 wing, Fig. 8, the picture for $\alpha = 8{\cdot}1$ deg shows the effect of the vortex sheet above the curved tip fairing, associated with separation at the extreme tip. On wing C a comparable stage of development is not reached until $\alpha = 12{\cdot}2$ deg (Fig. 9). On the RAE 101 wing the region of laminar separation extends down the leading edge with increase of incidence, accompanied by the associated vortex sheet, until at $\alpha = 16{\cdot}3$ deg most of the leading edge is affected and the vortex sheet springs from near the wing root. On wing C at this incidence, however, there is attached flow over the whole of the straight part of the leading edge and also apparently part of the way round the curved tip leading edge, and the vortex sheet is confined to the region of the tip fairing. Even at $\alpha = 22{\cdot}3$ deg, the flow over the forward part of the chord on wing C is attached over the inner two-thirds of the span. If the RAE 101 wing had been tested to such a high incidence it would almost certainly have shown leading-edge separation to exist over the whole span, with a full-chord separation on much of the outer wing. Without analysing the pictures in detail it is thus clear that they confirm that the improved pitching-moment characteristics of the drooped wings are the result of the droop and nose-thickening having considerably delayed the appearance and inward spread of flow separation near the leading edge.

Before leaving the subject of flow behaviour there are some interesting features of the flow over the drooped wings which have been absent or less noticeable in other tests, and these are discussed below before dealing with the force characteristics at higher Reynolds numbers on which they have some bearing.

(*a*) *Vortex sheet formation*

The flow studies on wing C did not show* the usual rolled-up or conical vortex sheet lying diagonally across the wing behind a leading-edge separation, as on the RAE 101 wing* and most other highly-swept wings[6]. Such a vortex would not in fact be expected, since as noted above leading-edge separation is absent on wing C except near the tip, and even there the flow remains attached for part of the way round the blunt nose, Fig. 9. However, the force results exhibit the usual characteristics of a part-span vortex sheet, *e.g.*, the nose-down moment change between $C_L = 0{\cdot}7$ and $C_L = 1{\cdot}0$ (Fig. 3), the accompanying increase in $dC_L/d\alpha$ (Fig. 4) and the reduction in the rate of inward movement of the spanwise centre of load (Fig. 6). Such a sheet is therefore believed to be present, but in a different form from usual because of the change from the long-bubble to the burst-short-bubble type of separation produced by the nose droop.

In two-dimensional flow the long bubble develops gradually with incidence, as already noted, whereas the short bubble 'bursts' suddenly to give a discontinuous change in pressure distribution and lift curve slope. On a sweptback wing, therefore, the bursting of a short bubble can be expected to cause a discontinuous change in flow conditions at the critical spanwise station, from attached flow on the inboard side to a severe separation immediately outboard, whereas the long bubble type of separation increases gradually in severity towards the tip. The diagonal vortex sheet usually found corresponds to the gradually increasing 'bubble size' of a long-bubble type separation towards

* The apparent resemblance in Figs. 8 and 9 between the flow over much of the rear part of wing C and the RAE 101 wing is deceptive. During the test runs it was obvious that the spanwise oil flow on the RAE 101 wing was due to the typical scouring action of a diagonal vortex sheet, evidence of which can be seen in the 'early' pictures for $\alpha = 14{\cdot}2$ deg and $\alpha = 16{\cdot}3$ deg. On wing C, however, there was no such scouring and the oil drifted spanwise quite slowly, as can be seen from Fig. 9. It is also perhaps worth noting that on the RAE 101 wing, as pointed out in Ref. 1, the usual flow pattern near the leading edge, associated with a long-bubble type separation and diagonal vortex sheet, is obscured inboard of $0{\cdot}4 \times$ semi-span by vortices shed from small surface imperfections near the leading edge.

the tip, and the corresponding redistribution of bound vorticity from front to rear of the outer sections; it is formed by the deformation of the separated shear layer into something approaching the conical vortex sheet found on more highly-swept planforms[9]. With a burst short bubble, on the other hand, the sheet can be expected to be more of the kind discussed in Ref. 20, standing up from the surface to form the more-or-less chordwise inboard boundary of the outer-wing separation cavity, and corresponding to the concentrated shedding of bound vorticity from the section at which the breakdown occurs. On this basis, the line dividing the region of no oil flow, near the tip, from the spanwise flow farther inboard, is thought to correspond roughly with the foot of the vortex sheet on wing C.

(*b*) *Spanwise sub-boundary layer*

The flow pictures for wing C provide an interesting visualization of the spanwise sub-layer on a swept wing at incidence. As noted in Refs. 8 and 9, spanwise curvature of the streamlines causes the flow nearest the surface to curve to a greater extent because of the smaller inertia forces, so that at some chordwise position the flow nearest the surface is directed purely towards the tip. Behind this point the boundary layer comprises a spanwise sub-layer thickening towards the trailing edge and the wing tip, with the chordwise boundary layer flowing over the top of it. The chordwise layer is in a sense separated, although the effects of such separation are generally much less severe than for a turbulent rear separation on an unswept wing. The 'line of separation'[19] of the chordwise layer is clearly shown in Fig. 9 by the line dividing the dark highly-scoured area on the front part of the wing from the area of thick slowly-flowing oil behind it. The pictures also show how the surface flow on the front part of the wing turns gradually spanwise with the line of separation forming the envelope of the flow lines, as discussed in Ref. 19.

(*c*) *Bursting of the bubble*

It has been suggested[10] that the change in two-dimensional flow from a short bubble to a long bubble or to a burst short bubble, as incidence increases, may be caused by a somewhat different mechanism from the generally accepted one put forward by von Doenhoff[1]. According to Ref. 10, instead of the bubble bursting because of the inability of the separated shear layer to reattach by turbulent mixing, it may burst because of the forward encroachment of a turbulent separation occurring just behind it. The distinction is perhaps not of great practical importance two-dimensionally but it may well be important on sweptback wings on which there is a spanwise sub-layer, as noted above. The flow pictures on wing *C** appear to lend some support to the ideas of Ref. 10, since it will be observed that at the highest incidences the inboard end of the tip leading-edge separation coincides with the point at which the 'line of separation' of the chordwise layer meets the short bubble. (The position of the bubble is shown by the white oil line just behind the leading edge.) For incidences and spanwise positions where the line of separation has not come forward to the bubble position the bubble remains intact. It is possible, on this basis, that the tip leading-edge separation may have occurred earlier in incidence because of the forward encroachment of the spanwise sub-layer. If so, there may be more to be gained by attacking the spanwise outflow (*e.g.*, by means of fences) than by further increasing the amount of nose droop and thickening compared with wing C.

3.1.3. *Effect of increasing Reynolds number to* 6×10^6. *On the RAE* 101 *wing* the increase of Reynolds number from 2×10^6 to 6×10^6 gives a C_L for final loss of stability of 0·85, an increase of

* And on the NACA 3 wing, Fig. 10.

0·2 (Fig. 3). There are similar increases in the C_L at which the drag starts to rise relatively steeply, Fig. 5, and at which the spanwise centre of load moves inward, Fig. 6. As discussed in Ref. 2, the improvement is attributable to a favourable scale effect on the local lift coefficient ($C_{L\,\mathrm{crit}}$ of Ref. 2) at which the long-bubble type of separation first appears at any given spanwise station. Fig. 3 shows that there is much less scale effect between $R = 4 \times 10^6$ and $R = 6 \times 10^6$ than between $R = 2 \times 10^6$ and $R = 4 \times 10^6$. Because of this, and because the value of $C_{L\,\mathrm{crit}}$ at $R = 6 \times 10^6$ is already of the order of 1·0, Ref. 2 concludes that little further scale effect is to be expected beyond $R = 6 \times 10^6$ provided that the stall remains due to leading-edge laminar separation. It is also stated in Ref. 2 that there might be no marked change in the overall behaviour even if, at higher Reynolds numbers, the character of the stall changed, *e.g.*, from laminar to turbulent separation. While the first conclusion is a valid one it now seems possible, in view of the results to be discussed below for the drooped wings, that further scale effect might in fact occur on the RAE 101 wing as a result of a change from laminar to turbulent separation at high Reynolds number.

On wings B *and* C the most noticeable feature of the results at higher Reynolds numbers is the adverse scale effect on the C_L for final loss of stability. On wing C, for instance, Fig. 3 shows that the C_L for loss of stability falls from 1·0 or 1·1 at $R = 2 \times 10^6$, depending how the curve is interpreted, to only 0·88 at $R = 6 \times 10^6$. This deterioration with R is accompanied by an earlier rise of drag, Fig. 5, an earlier inward movement of the spanwise centre of load, Fig. 6, and some reduction in lift beyond $C_L = 1{\cdot}0$, Fig. 4. It is therefore clearly the result of earlier or more severe flow separation on the outer sections at high Reynolds number. As a result of this adverse scale effect on the drooped wings, coupled with the favourable scale effect on the basic wing, wing C gives practically no increase in the C_L for loss of stability at $R = 6 \times 10^6$ whereas at $R = 2 \times 10^6$ it gave an increase of between 0·35 and 0·45 as already seen. The instability is less severe than on the RAE 101 wing, however.

Because of the absence of flow pictures for the drooped wings at high R the reasons for this unusual scale effect cannot be definitely established. It is thought, however, that at $R = 6 \times 10^6$ leading-edge laminar separation may be almost absent on wings B and C because of the amount of nose droop and thickening applied, in which case the flow breakdown may consist mainly of a turbulent rear separation such as occurs on thicker wings. In support of this is the fact that the pronounced nose-down moment change which precedes the instability at $R = 2 \times 10^6$, and which is known to be due to the vortex sheet associated with the tip leading-edge separation, is largely absent at $R = 6 \times 10^6$. This is as would be expected with a turbulent rear separation developing gradually towards the tip. Also, in the flow pictures at $R = 2{\cdot}6 \times 10^6$, Fig. 9, the flow near the outer-wing trailing edge for incidences of 14 deg or more has a marked forward component relative to the trailing edge, indicating a rear separation of both spanwise and chordwise boundary layers. In the absence of the vortex sheet due to the front separation this rear separation would probably spread farther forward; the vortex sheet effectively acts as a barrier to its forward movement by deflecting the surface flow rearward to near the tip trailing edge, Fig. 9. Although the rear separation is not evident below $\alpha = 14$ deg, the boundary-layer thickening which precedes it is thought to be the reason for the gradual increase of C_m and inward movement of the centre of load at lower incidences noted in Section 3.1.1.

On this basis, one explanation for the adverse scale effect on wing C may be that at high Reynolds numbers, where the separation is of the rear turbulent kind, instability occurs earlier due to loss of the favourable influence of the part-span vortex sheet associated with the tip leading-edge

separation. Thus, on a sweptback wing it may be more advantageous to have a leading-edge separation than to suppress it and have instead a rear turbulent separation. This is not particularly remarkable; a well-known example of the same sort of thing is provided by the slender delta planform, on which the vortex sheets dominate the flow and give a higher lift than would exist even in unseparated conditions.

Accepting the suggested changeover to a rear separation by $R = 6 \times 10^6$, another reason for the adverse scale effect is thought to be the additional spanwise outflow on the upper surface, caused by flow through the wing-root gap associated with the 'nett wing' technique. This is discussed further in Section 3.3.2 where it is suggested as the reason for the poor showing of the NACA 3 wing compared with American results.

In an attempt to reduce the tendency to rear separation, wing C was tested with a rear upper-surface fence at $0{\cdot}56 \times$ semi-span, Fig. 1, and the results are shown in Fig. 11. The fence largely eliminates the gradual increase in C_m at moderate incidences referred to above, and increases the C_L for instability at both $R = 2 \times 10^6$ and $R = 6 \times 10^6$. However, even with the fence there is instability below $C_{L\,\max}$ at the higher Reynolds number, and the adverse scale effect is still present. Better results at $R = 6 \times 10^6$ might be achieved with a full-chord fence or with the fence positioned nearer the tip, or it may be necessary to use more than one fence.

It is possible that the adverse scale effect on wings B and C may occur also on the RAE 101 wing if the leading-edge separation is suppressed by increase of Reynolds number beyond the test limit of 6×10^6. In view of this, a reliable assessment cannot be made of the possible improvement due to the tested droop shapes at full-scale Reynolds numbers.

3.2. *Characteristics of the NACA* 3 *Wing at Low Mach Number. Comparison with wings* B *and* C. The flow patterns, Fig. 10, and the force characteristics, Fig. 3, for the blunt-nosed uncambered NACA 3 wing at Reynolds numbers of about 2×10^6 are qualitatively similar to those for the drooped wings B and C. Quantitatively, however, it is evident that a given stage of flow development is reached about 4 deg earlier in incidence, and the C_L for loss of stability at $R = 2 \times 10^6$ is only about $0{\cdot}8$ compared with $1{\cdot}0$ to $1{\cdot}1$ for wing C. This reflects the earlier bursting of the short bubble on the NACA 3 wing at this Reynolds number due to the absence of camber. The effect of the droop C camber on the calculated pressure distribution at $0{\cdot}75 \times$ semi-span at $\alpha = 20$ deg is shown in Fig. 7; the peak value of $(-Cp)$ is $9{\cdot}5$ for the NACA 3 section compared with only $4{\cdot}2$ for droop C, and the peak occurs nearer to the leading-edge.

There is little scale effect on the C_L for loss of stability on the NACA 3 wing, whereas on wing C there is the adverse scale effect already noted. As a result, at $R = 6 \times 10^6$ there is less difference between the two wings, the C_L for loss of stability being $0{\cdot}80$ for the NACA 3 wing compared with $0{\cdot}88$ for wing C. The variation in shape of the $C_m - C_L$ curves with Reynolds number, and the absence of any favourable scale effect, suggest that the NACA 3 wing, like wing C, is affected by the growth of a rear separation with increase of Reynolds number. The effects of this are less marked, however, probably because the leading-edge separation persists more on the NACA 3 wing because of its higher peak suction.

Compared with the basic RAE 101 *wing* the NACA 3 wing increases the C_L for loss of stability by about $0{\cdot}15$ at $R = 2 \times 10^6$, but gives no gain at $R = 6 \times 10^6$. The absence of improvement at $R = 6 \times 10^6$, despite the reduction in peak $(-Cp)$ from about 20 to $9{\cdot}5$ at $\alpha = 20$ deg, is attributable to the same causes as discussed above for the drooped wings.

3.3. *American Results on NACA 3 and Similar Sections.* The relatively small improvement from the use of the NACA 3 section in these tests is in contrast with the fairly large gains found in American tests. A comparison with the American results is given below, first in relation to the available two-dimensional evidence and then in relation to American swept-wing tests.

3.3.1. *Two-dimensional results.* Two-dimensional results for the NACA 1, 2, 3 and 4 series sections, all of thickness chord ratio 0·06, are given in Refs. 4 and 12. They show that at $R = 6 \times 10^6$ the NACA 3–006 section has a maximum lift coefficient of 1·20. For a 6 per cent RAE 101 section Ref. 13 indicates a maximum lift coefficient of about 0·85 at this Reynolds number; thus, at $t/c = 0{\cdot}06$ and $R = 6 \times 10^6$ the NACA 3 section has an advantage of about 0·35 in $C_{L\max}$ compared with an RAE 101 section. This is to be expected in view of the large difference in nose radius, and the shape of the $C_L - \alpha$ and $C_m - C_L$ characteristics in Refs. 14 and 15 demonstrate quite clearly the corresponding change from the long-bubble separation on RAE 101 to the short-bubble separation on NACA 3, as discussed earlier.

The increase of t/c to the 0·075 tested here might give a smaller improvement in $C_{L\max}$ on the NACA 3 section than on the RAE 101 section, because of the relatively larger nose radius of the former. For the RAE 101 section an increase of about 0·15 would be expected, based on Ref. 15. No figures are available for the NACA 3 series. However, even if $C_{L\max}$ for NACA 3–007·5 is taken to be no greater than for NACA 3–006, which is rather unlikely, there remains an advantage of 0·2 in favour of a NACA 3–007·5 section compared with a $7\frac{1}{2}$ per cent RAE 101 section. On two-dimensional evidence, therefore, the absence of any advantage in favour of the NACA 3 wing in the present swept-wing tests at $R = 6 \times 10^6$ is somewhat surprising.

3.3.2. *Swept wing tests.* Ref. 14 gives comparative results for NACA 2–006 and NACA 65A006 sections on a 45 deg swept wing of aspect ratio 4 and taper ratio 0·6. At $R = 6 \times 10^6$ the 2–006 section gave an increase of 0·35 in the C_L for instability compared with the 65A006 section, the values being 0·95 and 0·6 respectively. Since Ref. 12 indicates little difference in two-dimensional $C_{L\max}$ between NACA 2– and NACA 3– sections it can be assumed that a similar result would be found with a 3–006 section in place of the tested 2–006.

For direct comparison with the present tests the NACA results can be roughly adjusted for the planform differences using the systematic data of Ref. 15; these suggest an addition of 0·1 to the NACA results to make them appropriate to the planform used in the present tests. On this basis we have at $R = 6 \times 10^6$:

NACA tests (adjusted)		
Section	NACA 65A006	NACA 2–006
C_L for instability	0·70	1·05
RAE tests		
Section	$7\frac{1}{2}$ per cent RAE 101	NACA 3–007–5
C_L for instability	0·85	0·81

From this comparison it is clear that either the NACA tests on 2–006 gave an unrealistically high value of C_L, or else the present results on 3–007·5 are for some reason pessimistic, since in the NACA tests the change to the blunt-nosed section gives a gain of 0·35 in C_L whereas in the RAE

tests it has an adverse effect. Likewise, the change from the 6 per cent thick 65A section to the $7\frac{1}{2}$ per cent thick RAE 101 gives an *increase* of 0·15 whereas the change from 2–006 to 3–007·5 gives a *decrease* of 0·24.

The 0·15 increase between the 6 per cent NACA 65A section and the $7\frac{1}{2}$ per cent RAE 101 section is almost exactly what would be expected from Ref. 13. Also, the increase of 0·35 between 65A006 and 2–006 is consistent with the measured two-dimensional $C_{L\,\max}$ data. It must therefore be concluded that the inconsistency lies in the present results for the NACA 3 wing, which are too low.

The reason for the poor showing of the NACA 3 wing in the present tests cannot be definitely established from the available evidence. It is thought, however, to be connected with the half-model test technique. It has already been suggested that at $R = 6 \times 10^6$ the NACA 3 wing, in common with the drooped wings, suffers from a turbulent rear separation. In the RAE tests, using the 'nett wing' technique, there was a 0·15 inch gap around the wing-root junction with the body. This allowed some flow to take place from the wing lower surface to the upper surface, which appeared as a spanwise outflow on the upper surface. When the tip flow breakdown is due to a rear separation, as suspected, the extra accumulation of spanwise boundary-layer air near the tip from this cause can be expected to promote an earlier tip stall and hence a lower C_L for loss of stability. In the NACA tests such an effect was absent, the wing being virtually integral with the tunnel floor, with no body represented and no gap around the wing root.

The existence of such outflow with the nett wing technique was known from earlier tests. However, in these tests it was not found to have any marked effect on the overall results. It now seems evident that this was because the earlier wings all suffered from leading-edge flow breakdown, which was relatively unaffected by the extra spanwise outflow; in the present tests the application of sufficient nose droop or thickening to suppress the leading-edge separation has allowed the outflow to exert its full effect. The nett wing technique has now been discarded and any future half-model tests will be done with body attached, accepting the interference caused by the tunnel-floor boundary layer on the forces on the body.

3.4. *Summary of Conclusions from Low-Speed Tests.* Before dealing with the tests at high Mach numbers the low-speed results can be summarized as follows:

(i) Although the blunt-nosed NACA 3 section and the drooped and thickened sections B and C give appreciable increases in the C_L for instability compared with the RAE 101 section at $R = 2 \times 10^6$, the increases at $R = 6 \times 10^6$ are small or negative because of favourable scale effect on the RAE 101 wing and adverse scale effect on the other wings.

(ii) At low Reynolds numbers the gains arise from replacement of the long-bubble type of separation on the RAE 101 wing by a short-bubble type on the other wings, due to the nose droop and thickening. At $R = 6 \times 10^6$, however, the flow breakdown on the drooped and thickened wings is thought to be of the rear turbulent kind. The effects of this can be more adverse than those of a leading-edge separation because of the absence of a strong part-span vortex sheet.

(iii) At $R = 6 \times 10^6$ it seems possible that the results on the NACA 3 wing and on wings B and C may have been adversely affected by flow through the gap at the wing-body junction; better results for these sections might therefore be obtained with a more suitable model test technique.

(iv) The results for wings B and C are better than those for the NACA 3 wing, *i.e.*, nose-thickening plus camber is better than nose-thickening alone.

(v) Because of the uncertainties regarding scale effect and model test technique it is not possible to say what advantage there might be for the NACA 3 or drooped-nose sections under full-scale conditions.

4. *Results and Discussion for Mach Numbers of* 0·50 *to* 0·94. 4.1. *General Behaviour.* Fig. 12 compares the $C_m - C_L$ curves for the four wings at Mach numbers between 0·50 and 0·94 and a Reynolds number of $1{\cdot}7 \times 10^6$, and Fig. 13 shows the variation of C_D with M at constant values of C_L. Lift carpets are given in Fig. 14, and Fig. 15 gives examples of the spanwise movement of the centre of lift with C_L and Mach number.

Considering first the general behaviour of the pitching-moment characteristics with Mach number for all four wings, Fig. 12 is consistent with the view put forward in Ref. 2 and elsewhere that the Mach number range can be broadly subdivided into three regions as described below:

(i) *For Mach numbers up to about* 0·85 Figs. 3 and 12 show a gradual decrease in the C_L for instability as Mach number increases, the rate of decrease being greatest between $M = 0{\cdot}2$ and $M = 0{\cdot}5$. In this Mach number range the nature of the flow breakdown remains effectively the same as at low Mach numbers and $R = 2 \times 10^6$, lift being lost on the outer sections as a result of separation from near the leading-edge. At the higher Mach numbers the separation is induced by small shock waves[16] rather than by high suction peaks as at low speeds, but its effects on the pressure distribution are similar. Between $M = 0{\cdot}18$ ($R = 2 \times 10^6$) and $M = 0{\cdot}85$ the lift coefficients for loss of stability decrease as follows:

	$M = 0{\cdot}18$	$M = 0{\cdot}85$
RAE 101 wing	0·67	0·54
NACA 3 wing	0·82	0·46
Wing B	1·02	0·58
Wing C	1·0 to 1·1	0·58

(ii) *At Mach numbers between about* 0·85 *and* 0·90 there are increases in the values of C_L for loss of stability, and the loss of stability when it occurs is less marked than at lower Mach numbers. On the RAE 101 wing, for instance, the C_L for instability increases by about 0·1 between $M = 0{\cdot}85$ and $M = 0{\cdot}90$, and on the drooped wings there is no significant loss of stability up to $C_L = 0{\cdot}8$ or 0·9 at Mach numbers of 0·88 and 0·90, apart from the kinks near $C_L = 0{\cdot}4$, Fig. 12. The improvements in this intermediate speed range are due to the development of a supersonic expansion round the outer-wing leading-edge, as noted in Refs. 2, 17 and 18. This effectively* suppresses the leading-edge laminar separation and the breakdown, when it takes place, is due to the shock at the rear of the expansion. Fig. 16, taken from subsequent pressure-plotting results on the RAE 101 wing, illustrates some typical effects of the expansion on the pressures and local C_L near 0·72 × semi-span. The general effect is to delay the first onset of outer-wing separation compared with the trend at lower Mach numbers, and perhaps more important, to maintain higher

* A small bubble may exist beneath the expansion.

upper-surface suctions and higher lift coefficients after separation occurs. This type of improvement at intermediate Mach numbers has often been observed in two-dimensional tests, *e.g.*, in Ref. 18 where it is very marked.

(iii) *At Mach numbers of* 0·92, 0·94 this improvement comes to an end, and there is now a marked reduction of stability near $C_L = 0{\cdot}5$ on all the test wings, arising from a fairly severe shock-induced separation on the outer wing; similar but less well defined tendencies are also apparent at $M = 0{\cdot}88$, 0·90. At the higher Mach numbers the usable C_L would in practice almost certainly be limited to that for the sudden stability change, either by buffeting or by loss of stability with tail on, which is generally more severe than with tail off unless the tail is mounted sufficiently below the wing chord plane. The position at $M = 0{\cdot}88$, 0·90 is less clear.

Having noted these general characteristics on all four wings as Mach number is varied, the effects of the different wing sections will now be considered in more detail.

4.2. *Pitching-Moment Characteristics of the RAE* 101 *and the Drooped Wings.* Fig. 12 shows that except at low incidences, where wing C has more negative values of C_m due to its higher camber, the $C_m - C_L$ curves for wings B and C are very much alike. The lift curves, Figs. 14b and 14c, are also alike.

Compared with the basic RAE 101 wing, the drooped wings give appreciable improvements in pitching-moment characteristics at low and moderate Mach numbers, but their advantage decreases with increase of Mach number until at $M = 0{\cdot}92$, 0·94 they give no increase in the C_L for loss of stability.

At low and moderate Mach numbers the increase in the C_L for instability, and the reduction in severity of the instability when it occurs, are of course due to the effect of the nose droop and thickening in delaying the leading-edge separation, as already discussed. The marked decrease in advantage with increase of Mach number, from $\Delta C_L \sim 0{\cdot}35$ at $M = 0{\cdot}18$ to $\Delta C_L \sim 0{\cdot}05$ at $M = 0{\cdot}85$, is thought to be due in part to the considerable nose thickening incorporated in the droop design. This is advantageous at low speeds but probably causes the early formation of small shocks near the leading-edge at higher Mach numbers. The results, both absolute and comparative, in the lower part of this Mach number range, may be subject to considerable scale effect as discussed in Section 3. Beyond about $M = 0{\cdot}85$, however, this kind of scale effect should no longer occur, the separations then being of the rear shock-induced type.

At $M = 0{\cdot}88$, 0·90 the drooped wings retain more or less constant stability up to lift coefficients of 0·8 to 0·9, apart from the kink near $C_L = 0{\cdot}4$. The RAE 101 wing, on the other hand, loses stability beyond about $C_L = 0{\cdot}65$. Providing the limit on usable C_L is not set in practice by buffeting or tail-on instability at lower incidence—*e.g.*, near $C_L = 0{\cdot}4$—the drooped sections would appear to have a distinct advantage at these Mach numbers. Fig. 15a indicates that the better behaviour of the drooped wings compared with the RAE 101 wing beyond $C_L = 0{\cdot}65$ is due to the maintenance of higher lift coefficients on the outer wing sections. This is thought to be due to the favourable influence of the nose droop in retarding the forward spread of shock-induced separation with incidence at these Mach numbers, thereby maintaining the front suction peaks to higher incidences.

At $M = 0{\cdot}92$, 0·94 the limit on usable C_L is likely to be set by buffeting or tail-on instability at (or below) the lift coefficients at which the relatively large reductions of stability occur in Fig. 12.

The drooped wings do not appear to have any advantage at these Mach numbers, loss of stability occurring near $C_L = 0{\cdot}55$ in all cases. The absence of any improvement at the highest test Mach numbers is somewhat disappointing in view of the fact that, on the basic wing, pressure measurements have shown the loss of stability to be still caused by a forward spread of the shock-induced separation to near the leading-edge, as at $M = 0{\cdot}88$, $0{\cdot}90$ where the droop has a favourable influence.

In some unpublished tests, nose droop did in fact give appreciable improvements right up to $M = 0{\cdot}94$ by delaying the collapse of the leading-edge suctions. The droop used, however, differed from those tested here in that the thickness near the nose was reduced when droop was applied, instead of being considerably increased as in the present tests. The increase in nose thickness is the result of designing in the first place for the maximum improvement for take-off and landing, in the hope that some improvement would also be obtained at higher Mach numbers. It would seem that if improvements are required at high speeds, the droop must be designed for these speeds and nose thickening of the amount tested here must be avoided.

4.3. *Part-Span Droop.* The decision to investigate full-span droop arrangements was based on some relatively favourable results obtained with droop B applied only between $0{\cdot}56$ and $0{\cdot}89$ of the semi-span, with unfaired inboard and outboard extremities. The pitching-moment characteristics for this part-span droop are compared with the present results in Fig. 17. It can be seen that the full-span droop rather unexpectedly gives poorer results over most of the Mach number range from $M = 0{\cdot}50$ to $M = 0{\cdot}94$. *Between* $M = 0{\cdot}50$ *and* $M = 0{\cdot}85$ the C_L for the final loss of stability, disregarding the gradual increase in C_m at lower lift coefficients referred to earlier, is of the order of $0{\cdot}2$ smaller with the full-span arrangement. *At* $M = 0{\cdot}88$, $0{\cdot}90$ there is little difference at high C_L, but the part-span droop does not exhibit the stability changes present near $C_L = 0{\cdot}4$ with full-span droop. *At* $M = 0{\cdot}92$, $0{\cdot}94$ the full-span droop gives no advantage over the basic wing, as already noted. Part-span droop, however, gives an advantage of about $0{\cdot}1$ in C_L at $M = 0{\cdot}92$, and at $M = 0{\cdot}94$ it gives a smaller loss of stability beyond $C_L = 0{\cdot}5$.

Without pressure distributions or flow studies the reasons for the advantage of the part-span arrangement at high speeds cannot be established. The advantage is thought to be connected, however, with the discontinuities in thickness and leading-edge planform at the inner and outer ends of the droop, which generate part-span vortex sheets affecting the flow over the outer half of the wing. At low and moderate Mach numbers certainly, the vorticity shed from the inner discontinuity is known to have a favourable influence, both through its direct effect on the outer-wing lift coefficients and also by its indirect effect in acting as a barrier to the spanwise outflow from the inboard sections, in the same manner as a chord fence.

4.4. *Pitching-Moment Characteristics of the NACA 3 Wing.* As already noted, at $M = 0{\cdot}18$ and $R = 2 \times 10^6$ (Fig. 3) the NACA 3 section increases the C_L for instability by about $0{\cdot}15$ compared with the RAE 101 section. Fig. 12 shows that this fairly small improvement becomes still less as Mach number increases, and has almost vanished by $M = 0{\cdot}65$. At these fairly low Mach numbers the relative deterioration of the NACA 3 performance with increase of Mach number is probably due to the formation of small shock waves on the blunt nose, as suggested for the drooped sections.

Beyond $M = 0{\cdot}7$ the C_L for instability on the NACA 3 wing is smaller than on the RAE 101 wing, the difference being greatest at $M = 0{\cdot}9$ where it amounts to $0{\cdot}2$. The beneficial effects of

the supersonic expansion are absent on the NACA 3 section. This may be because the expansion is less extensive because of the nose shape, or it may be that the shock following the expansion gives a more severe separation than on RAE 101 due to its proximity to the far-forward maximum thickness position ($0{\cdot}18c$ against $0{\cdot}31c$ for RAE 101). None of the tests yet made on this type of section have included pressure distributions or flow studies at high speeds.

Comparison with the drooped wings shows that over the entire Mach number range the latter give higher values of the C_L for instability, presumably because of their camber—as Fig. 2 shows, their thickness distributions are not markedly dissimilar from that of the NACA 3 section. This, together with the adverse effect of nose-thickening alone, as just seen, lends support to the view that at high speeds better results are obtainable with nose droop alone than with a combination of droop and thickening as used here.

4.5. *Drag Characteristics.* Fig. 13 shows the variation of C_D with Mach number at various constant values of C_L for the four wings tested.

4.5.1. *Drag at* $C_L = 0$. At zero lift the NACA 3 wing and the wing with droop B have roughly equal drag coefficients, C_D for these wings being about $0{\cdot}0025$ higher than for the basic RAE 101 wing throughout the Mach number range $0{\cdot}50$ to $0{\cdot}94$. The drag divergence Mach number M_D (*i.e.*, where C_D has risen by $0{\cdot}005$ compared with its value at $M = 0{\cdot}5$) is outside the test Mach number range at $C_L = 0$.

So far as the NACA 3 wing is concerned, the increase of $0{\cdot}0025$ in C_D compared with the RAE 101 wing, at Mach numbers below M_D, is in reasonable agreement with such reliable NACA tests as have been made (some of the NACA results[12,14] are unreliable because of model asymmetry and insensitivity of the drag balance). The drag penalty is quite large, but part of the increase is probably the effect of a difference in transition position. On the NACA 3 section, transition would be expected to occur ahead of $0{\cdot}1c$ as a result of a forward suction peak calculated for this section at zero incidence[12]. With an RAE 101 section, however, tests on a 40 deg swept wing in Ref. 19 using the acenaphthene sublimation technique showed transition to be at about mid-chord at $C_L = 0$. A difference of $0{\cdot}4c$ in the position of transition would account for about $0{\cdot}0017$ of the measured $0{\cdot}0025$ increase in C_D for the NACA 3 section. A similar difference would be expected to exist between wing B and the basic RAE 101 wing, since droop B also gives a suction peak near the leading-edge at zero lift. Thus, in full-scale conditions where transition may be well forward for all three sections, the zero-lift drag penalty with either droop B or the NACA 3 section may be only of the order of $0{\cdot}001$ in C_D up to $M = 0{\cdot}94$.

With droop C the measured drag penalty at $C_L = 0$ is appreciably higher than for droop B or the NACA 3 wing, particularly at high Mach numbers. At $M = 0{\cdot}9$, for instance, the value of C_D is practically doubled, from $0{\cdot}007$ to $0{\cdot}013$, by using droop C.

4.5.2. *Drag for* $C_L > 0$. At low Mach number (*e.g.*, $M = 0{\cdot}5$, Fig. 13) the drag of the RAE 101 wing increases fairly rapidly with increase of C_L as a result of the leading-edge flow separation. The other three sections tested delay and reduce the extent of the separation, and so at some C_L their drag becomes less than that of the basic wing; at $M = 0{\cdot}5$ this is the case beyond about $C_L = 0{\cdot}3$, the improvement being largest for the drooped wings. With increase of Mach number the improvement in drag at moderate and high C_L diminishes, until at $M = 0{\cdot}9$ the drag of the drooped wing is about the same as that of the RAE 101 wing beyond $C_L = 0{\cdot}4$, and that of the NACA 3 wing is considerably greater.

Comparing the symmetrical NACA 3 wing with the better of the two drooped wings, wing B, Fig. 13 shows that at moderate and high lift coefficients the NACA 3 wing has appreciably greater drag at all Mach numbers. At $C_L = 0$, as already noted, the two sections are about equal. Thus, so far as drag is concerned the droop B section is preferable to the symmetrical NACA 3 section at all test incidences and Mach numbers. This conclusion is in the same sense as that reached in Section 4.4 with respect to the pitching-moment characteristics. Thus, from all points of view it seems that nose droop is more advantageous than nose thickening, and there is no case for the use of sections of the symmetrical NACA 3 kind on this type of wing.

5. *Conclusions.* From the tests at low Mach number, varying Reynolds number, the principal conclusions are:

(i) Although the blunt-nosed NACA 3 section and the drooped sections, B and C, increase the C_L for instability compared with an RAE 101 section at $R = 2 \times 10^6$, the gains at $R = 6 \times 10^6$ are small or negative, there being a favourable scale effect on the RAE 101 wing and an unusual adverse scale effect on the modified wings.

(ii) The gains at $R = 2 \times 10^6$ are thought to be due to a change in the nature of the leading-edge separation from long-bubble type on the RAE 101 wing to short-bubble type on the modified wings. At $R = 6 \times 10^6$, however, it is suggested that turbulent rear separation occurs on the modified wings, the effects of which may be more adverse than those of a leading-edge separation because of the absence of a strong part-span vortex sheet.

(iii) The results for the modified wings at $R = 6 \times 10^6$ may have been adversely affected by flow through a gap at the wing-body junction associated with the 'nett half-wing' technique.

The tests at high Mach numbers show that:

(i) The improvement in the value of C_L for instability (at $R = 2 \times 10^6$) due to nose thickening or droop decreases with increase of Mach number. The drooped wings give no advantage over the basic RAE 101 wing beyond about $M = 0{\cdot}9$, and the NACA 3 wing is worse than the RAE 101 beyond about $M = 0{\cdot}7$.

(ii) The thickened nose is clearly disadvantageous at high speeds, and from these and other tests it seems likely that better results would be obtained from the use of nose droop without any thickening, or even with a sharper nose.

(iii) The drooped-nose sections are better than the symmetrical NACA 3 section in respect of both drag and pitching-moment characteristics throughout the test Mach number range.

(iv) Comparing the present droop results with those of Ref. 1, it appears that at high Mach numbers droop on the outer wing only, with a leading-edge discontinuity at its inboard end, gives better results than a full-span droop with no discontinuity.

REFERENCES

No.	*Author(s)*	*Title, etc.*
1	A. B. Haines	The subsonic characteristics at high C_L of wings with 50 deg sweep and 7·5 per cent thick sections, and the effectiveness of various devices to improve these characteristics. A.R.C. 17,145. August, 1954.
2	A. B. Haines and C. W. Rhodes ..	Tests in the R.A.E. 10 ft × 7 ft High Speed Tunnel on three wings with 50 deg sweepback and 7·5 per cent thick sections. A.R.C. R. & M. 3043. September, 1954.
3	A. B. Haines and C. W. Rhodes ..	Tests in the R.A.E. 10 ft × 7 ft High Speed Tunnel on a 7·5 per cent thick 50 deg swept wing fitted with stall fences and a leading-edge chord extension. A.R.C. R. & M. 3043. September, 1954.
4	L. K. Loftin and A. E. von Doenhoff	Exploratory investigation at high and low subsonic Mach numbers of two experimental 6 per cent thick airfoil sections designed to have high maximum lift coefficients. N.A.C.A. Research Memo. L51F06. TIB 2966. December, 1951.
5	A. B. Haines	Some notes on the flow patterns observed over various swept-back wings at low Mach number in the R.A.E. 10 ft × 7 ft High Speed Tunnel. A.R.C. R. & M. 3192. September, 1954.
6	G. G. Brebner	The application of camber and twist to swept wings in incompressible flow. A.R.C. C.P.171. March, 1952.
7	J. Weber	The calculation of the pressure distribution on the surface of thick cambered wings and the design of wings with given pressure distributions. A.R.C. R. & M. 3026. June, 1955.
8	D. Küchemann	A non-linear lifting-surface theory for wings of small aspect ratio with edge separations. A.R.C. 17,769. April, 1955.
9	D. Küchemann	Boundary layers on swept wings; their effects and their measurement. Unpublished M.O.A. Report.
10	R. A. Wallis	Experiments with air jets to control the nose stall on a 3 ft chord NACA 64A006 aerofoil. A.R.C. 17,311. January, 1955.
11	A. von Doenhoff	A preliminary investigation of boundary layer transition along a flat plate with adverse pressure gradient. N.A.C.A. Tech. Note 639. March, 1938.
12	N. J. Paradiso	Investigation at high and low subsonic Mach numbers of two symmetrical 6 per cent thick airfoil sections designed to have high maximum lift coefficients at low speeds. N.A.C.A. Research Memo. L52I02. TIB 3433. October, 1952.

REFERENCES—*continued*

No.	*Author(s)*	*Title, etc.*
13	I. H. Abbot and A. von Doenhoff . .	*Theory of wing sections.* McGraw Book Co. Inc. 1949.
14	S. F. Racisz and N. J. Paradiso . .	Wind tunnel investigation at high and low subsonic Mach numbers of a thin sweptback wing having an airfoil section designed for high maximum lift. N.A.C.A. Research Memo. L51L04. TIB 3021. February, 1952.
15	J. F. Cahill and S. M. Gottlieb . .	Low-speed aerodynamic characteristics of a series of swept wings having NACA 65A006 airfoil sections. N.A.C.A. Research Memo. L50F16. TIB 2555. October, 1950.
16	H. H. Pearcey and M. E. Faber . .	Detailed observations made at high incidences and high subsonic Mach numbers on a Goldstein 1442/1547 aerofoil. A.R.C. R. & M. 2849. November, 1950.
17	H. H. Pearcey	The occurrence and development of boundary layer separations at high incidences and high speeds. A.R.C. R. & M. 3109. September, 1955.
18	W. F. Lindsey and E. J. Landrum . .	Force and flow characteristics of 2 per cent thick airfoils at transonic speeds. N.A.C.A. Research Memo. L54I30. TIB 4548. January, 1955.
19	E. C. Maskell	Flow separation in three dimensions. A.R.C. 18,063. November, 1955.
20	D. Küchemann	Types of flow on swept wings with special reference to free boundaries and vortex sheets. A.R.C. 15,756. March, 1953.

TABLE 1

Leading Dimensions of Models

*Half wings**

Section		RAE 101 NACA 3	Droop B	Droop C
Gross area (C_L to tip)	ft²	3·395	3·460	3·480
Nett area (root chord to tip)	ft²	2·804	2·858	2·875
Gross mean chord	in.	17·78	18·12	18·22
Nett mean chord	in.	16·77	17·09	17·19
Centre-line chord	in.	26·08	26·56	26·71
Root chord	in.	24·02	24·48	24·62
Tip chord (projected, *i.e.*, with L.E. continued straight to tip)	in.	9·44	9·62	9·68
Span	in.	27·5	27·5	27·5
Aspect ratio		3·10	3·04	3·02
Taper ratio (based on projected tip chord)		0·362	0·362	0·362
Sweepback of quarter-chord line	deg	50	50·2	50·3
Thickness/chord ratio		0·075	0·075	0·075
Distance of nett mean quarter-chord point behind L.E. C_L chord	in.	22·86	23·10	23·18

Half body

Half-width (*i.e.*, in spanwise direction)	in.	3·4
Depth (*i.e.*, in plane of symmetry)	in.	2·0
Length	in.	70·0

* Area, mean chord and aspect ratio are based on a square tip having the projected tip chord, rather than the curved tip, as in previous reports of this series.

TABLE 2

Section Ordinates

cx Chordwise distance aft of L.E. of basic RAE 101 section.

cZ_u Upper-surface ordinate, measured from undrooped chord-line.

cZ_L Lower-surface ordinate, measured from undrooped chord-line.

c Chord length of basic undrooped section.

(Z_u is positive upwards, Z_L is positive downwards).

	Droop 'C'		Droop 'B'		RAE 101	NACA 3–007·5	
$100x$	$100Z_u$	$100Z_L$	$100Z_u$	$100Z_L$	$100Z_u$, Z_L	$100x$	$100Z_u$, Z_L
−2·5	−3·15	3·15					
−2·3	−2·02	3·66					
−2·1	−1·61	3·90					
−1·9	−1·29	4·04	−2·00	2·00			
−1·7	−1·03	4·15	−1·21	2·50			
−1·5	−0·80	4·23	−0·85	2·72			
−1·3			−0·60	2·87			
−1·0	−0·31	4·36	−0·31	3·04			
−0·5	0·10	4·45	0·10	3·24			
0	0·42	4·49	0·42	3·40	0	0	0
0·5	0·69	4·52	0·69	3·50	0·65	0·52	1·08
1	0·92	4·56	0·92	3·61	0·92	2·08	2·06
2	1·29	4·57	1·29	3·75	1·29		
3	1·57	4·58	1·57	3·85	1·57		
5	2·00	4·57	2·00	3·97	2·00	4·68	2·85
7·5	2·39	4·53	2·39	4·03	2·39	8·31	3·40
10	2·70	4·49	2·70	4·04	2·70	12·93	3·69
15	3·16	4·34	3·16	4·03	3·16	18·48	3·75
20	3·47	4·20	3·47	4·01	3·47	20	3·75
25	3·66	4·06	3·66	3·96	3·66	25	3·72
30	3·74	3·90	3·74	3·87	3·74	30	3·65
35	3·72	3·76	3·72	3·74	3·72	35	3·55
40	3·60	3·60	3·60	3·60	3·60	40	3·42
50	3·20	3·20	3·20	3·20	3·20	50	3·07
60	2·65	2·65	2·65	2·65	2·65	60	2·62
70	2·01	2·01	2·01	2·01	2·01	70	2·08
80	1·34	1·34	1·34	1·34	1·34	80	1·46
90	0·67	0·67	0·67	0·67	0·67	90	0·79
100	0	0	0	0	0	100	0·07

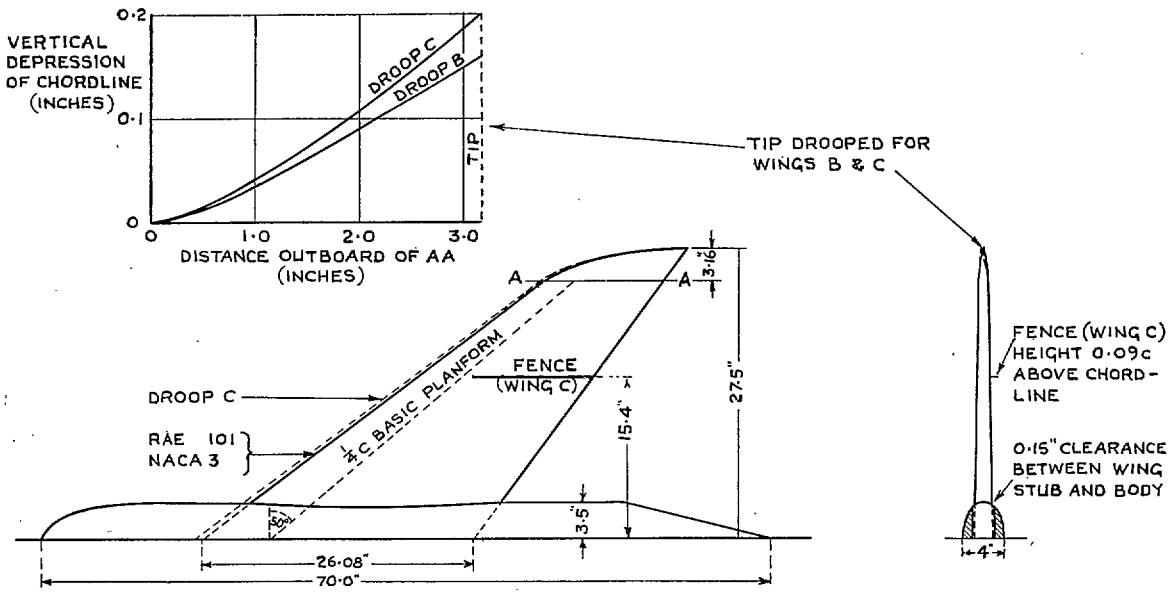

FIG. 1. General arrangement of models (Section 2.1).

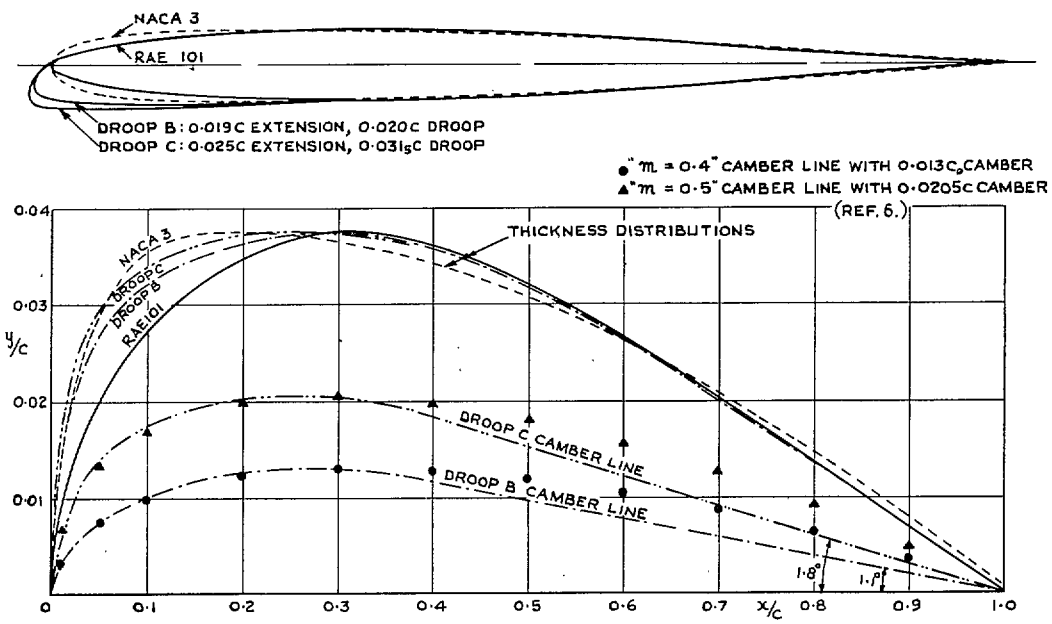

FIG. 2. Comparison of wing section shapes (Section 2.2).

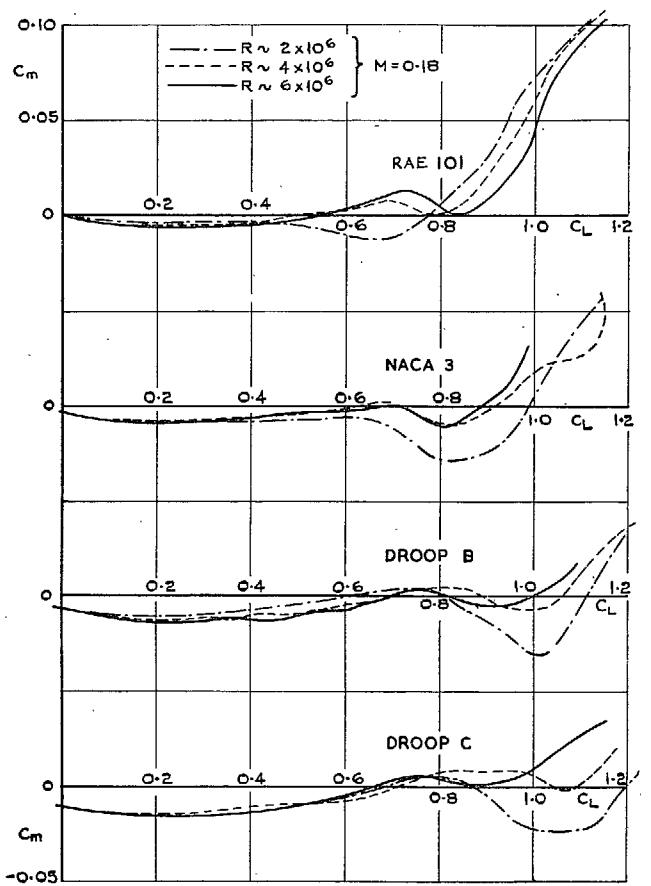

FIG. 3. C_M vs. C_L at low Mach number. Effect of section shape and Reynolds number (Sections 3.1, 3.2).

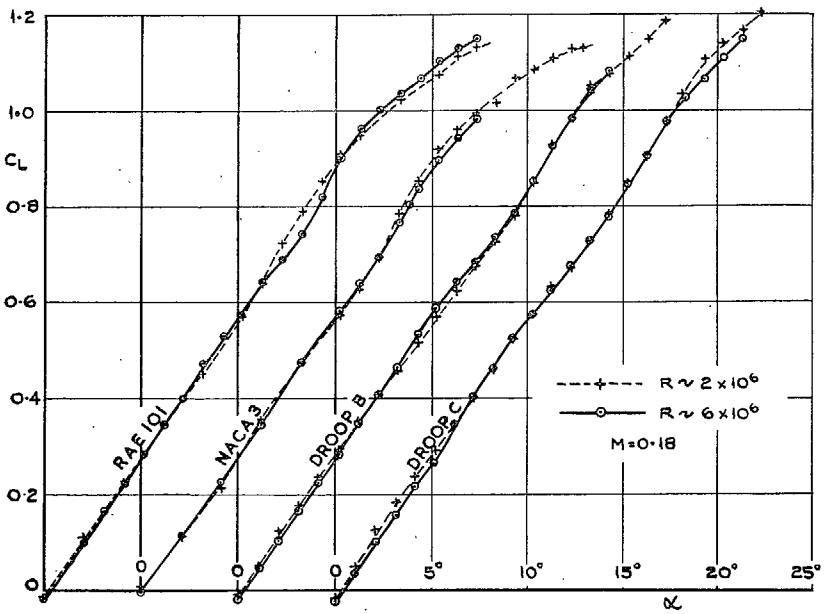

FIG. 4. Comparison of $C_L - \alpha$ curves at low Mach number. Effect of section shape and Reynolds number (Sections 3.1, 3.2).

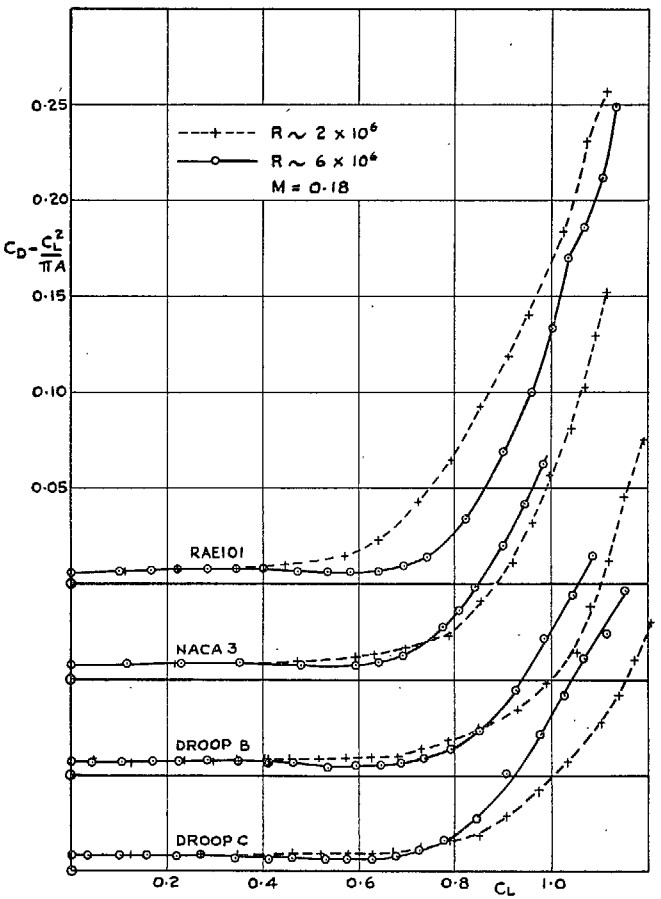

FIG. 5. $C_D - C_L^2/\pi A$ vs. C_L at low Mach number. Effect of section shape and Reynolds number (Sections 3.1, 3.2).

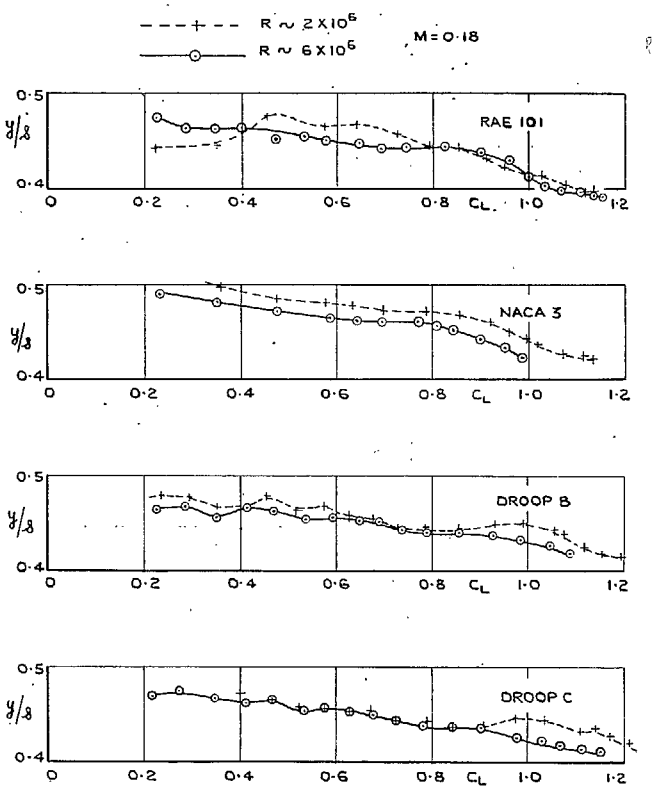

FIG. 6. Spanwise centre of load at low Mach number. Effect of section shape and Reynolds number (Sections 3.1, 3.2).

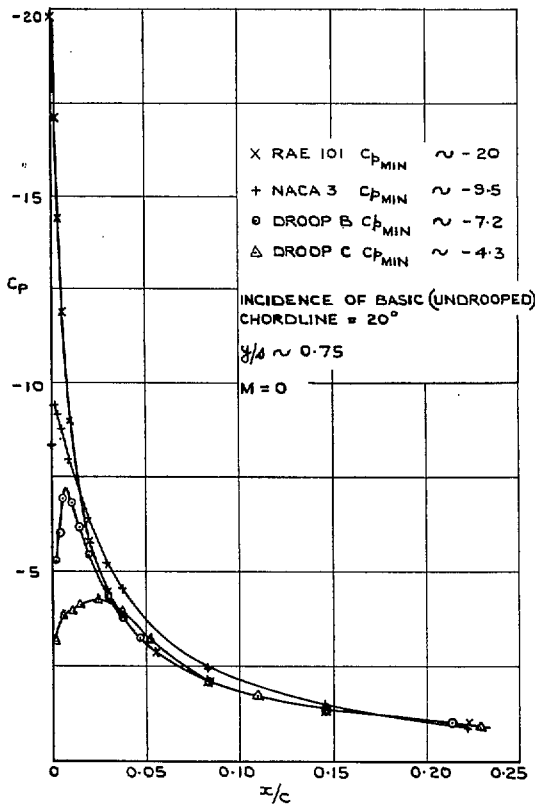

FIG. 7. Comparison of calculated upper-surface pressure distributions on front part of chord at $\alpha = 20$ deg, $y/s \sim 0{\cdot}75$, $M = 0$ (Sections 3.1, 3.2).

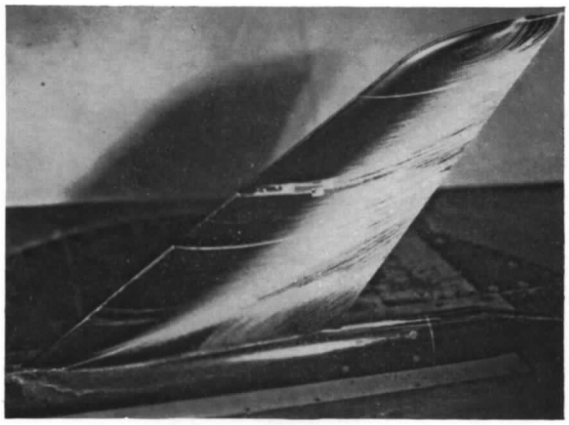

$\alpha = 8.1^{\circ}$ early

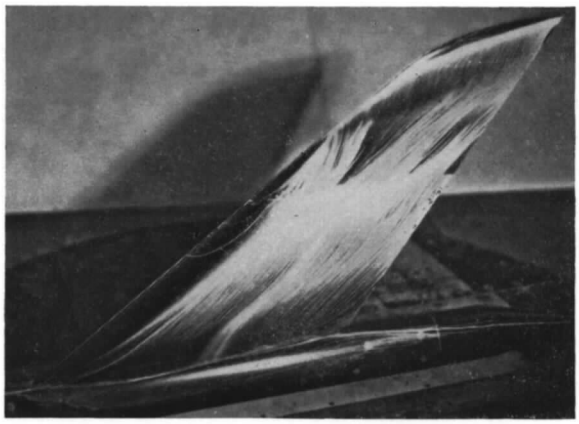

$\alpha = 12.2^{\circ}$ early

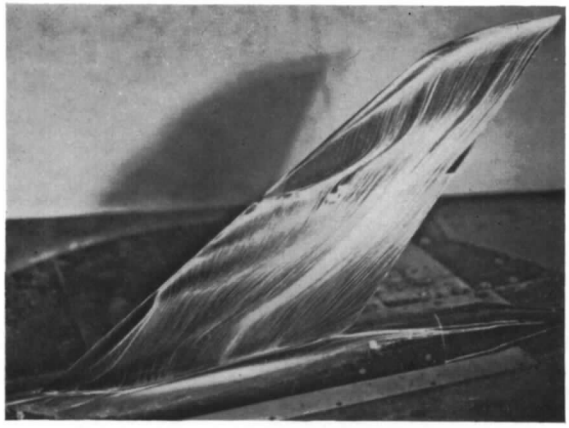

$\alpha = 14.2^{\circ}$ early

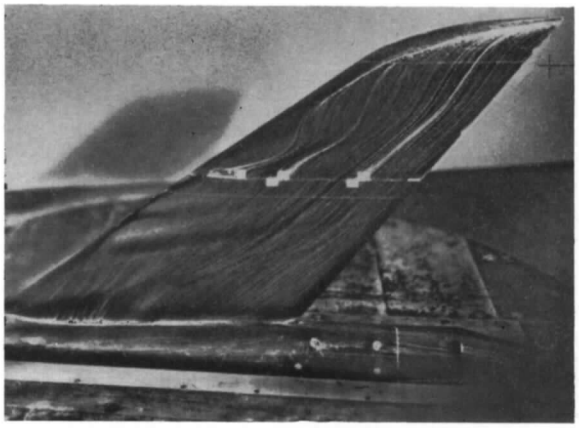

$\alpha = 14.2^{\circ}$ final

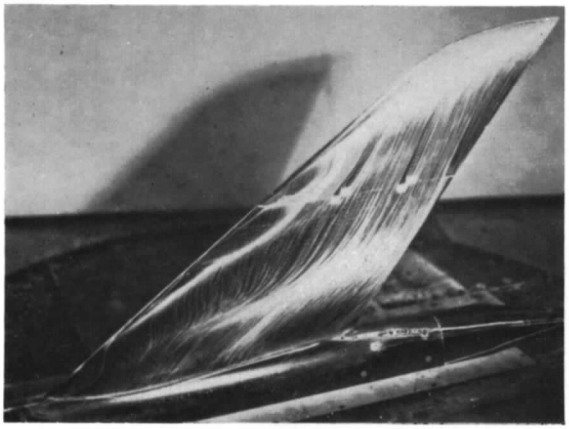

$\alpha = 16.3^{\circ}$ early

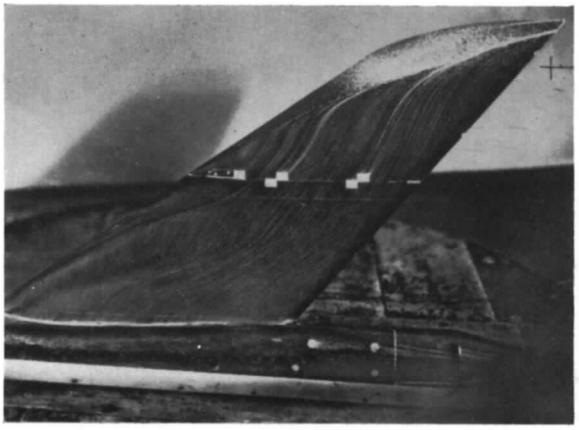

$\alpha = 16.3^{\circ}$ final

FIG. 8. Flow patterns, RAE 101 wing. $R = 2{\cdot}6 \times 10^6$, $M = 0{\cdot}27$ (Section 3.1.2).

$\alpha = 12.2^{\circ}$

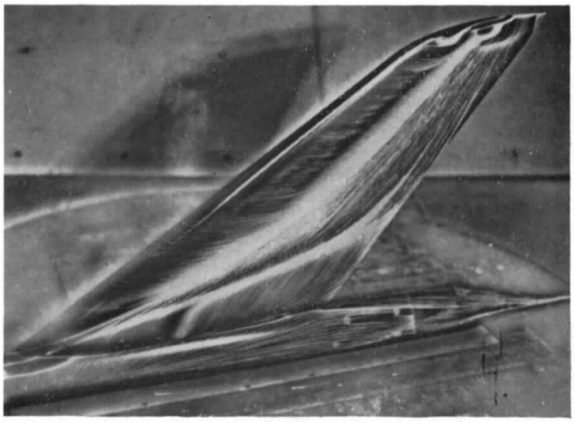

$\alpha = 14.2^{\circ}$

$\alpha = 16.3^{\circ}$

$\alpha = 18.3^{\circ}$

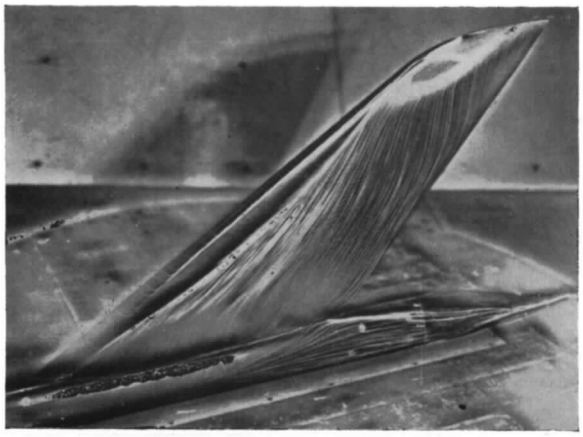

$\alpha = 20.3^{\circ}$

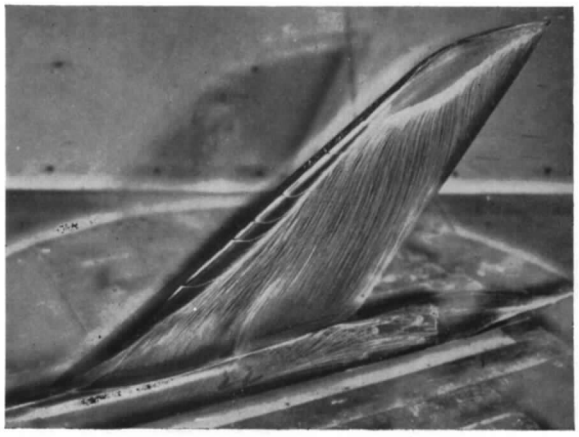

$\alpha = 22.3^{\circ}$

FIG. 9. Flow patterns, droop 'C'. $R = 2{\cdot}6 \times 10^6$, $M = 0{\cdot}27$ (Section 3.1.2).

$\alpha = 12.2^{\circ}$

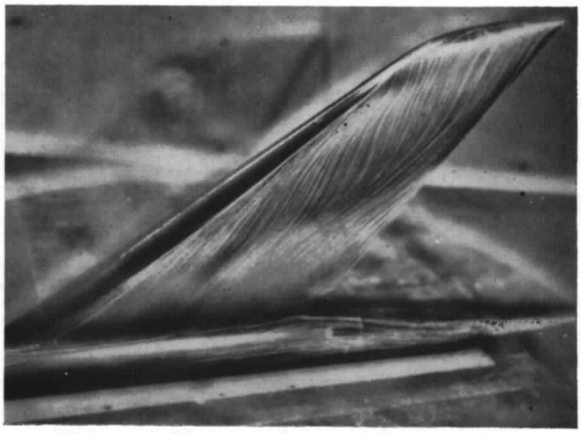

$\alpha = 14.2^{\circ}$

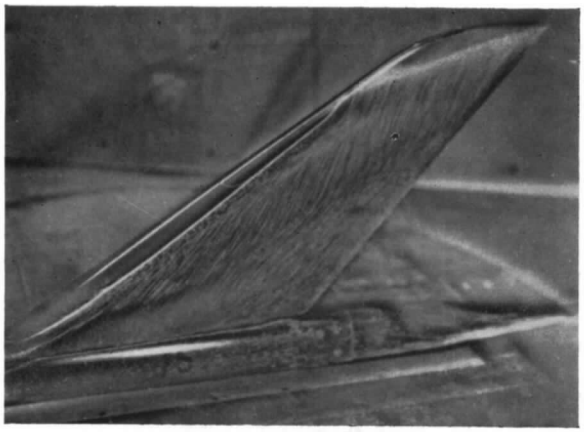

$\alpha = 15.2^{\circ}$

$\alpha = 16.3^{\circ}$

$\alpha = 18.3^{\circ}$

$\alpha = 20.3^{\circ}$

FIG. 10. Flow patterns, NACA '3' wing. $R = 2{\cdot}6 \times 10^6$, $M = 0{\cdot}27$ (Section 3.2).

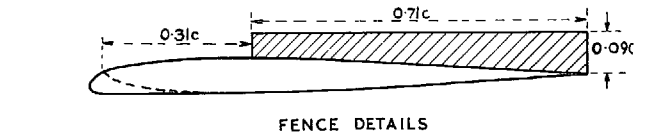

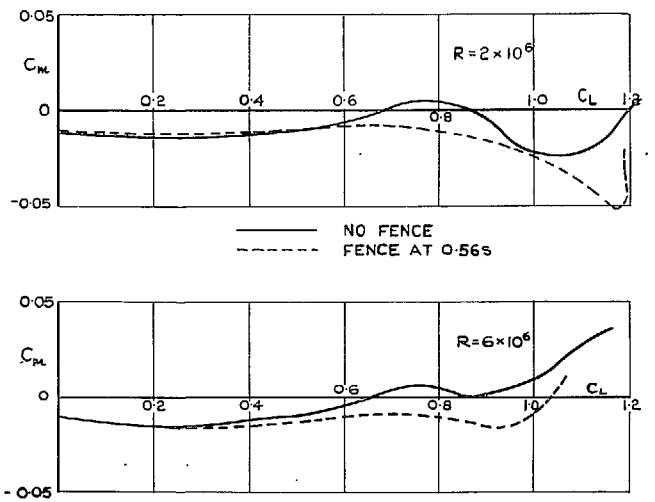

FIG. 11. Effect of upper-surface fence on $C_m - C_L$ characteristics of wing C at $M = 0{\cdot}18$ (Section 3.1.3).

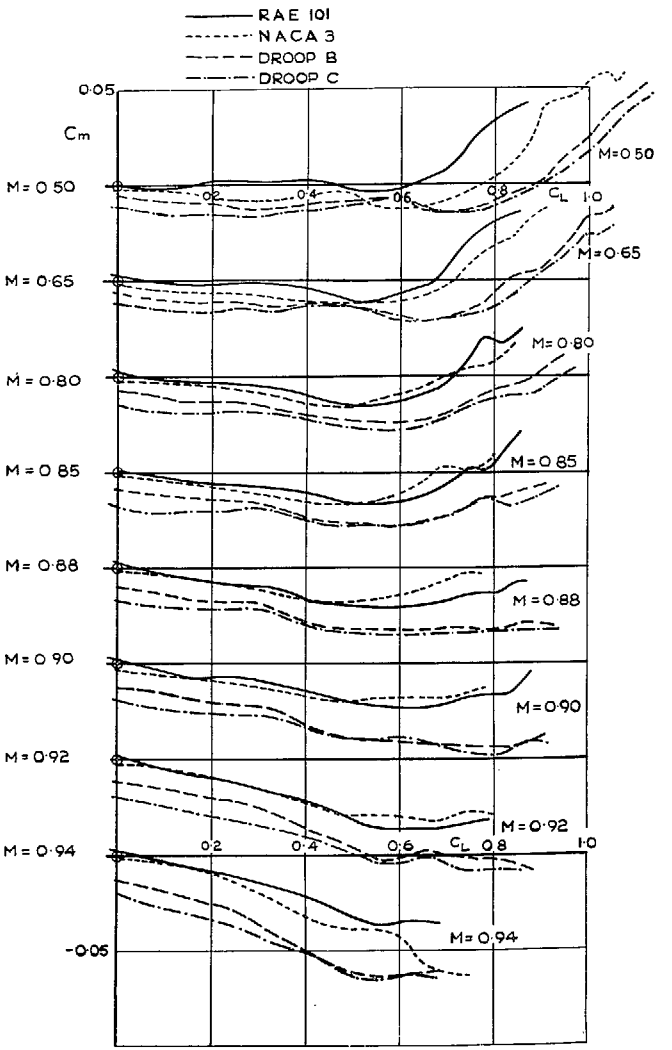

FIG. 12. C_m vs. C_L at various Mach numbers. Effect of section shape. $R \sim 1{\cdot}7 \times 10^6$ (Sections4. 1, 4.2, 4.4).

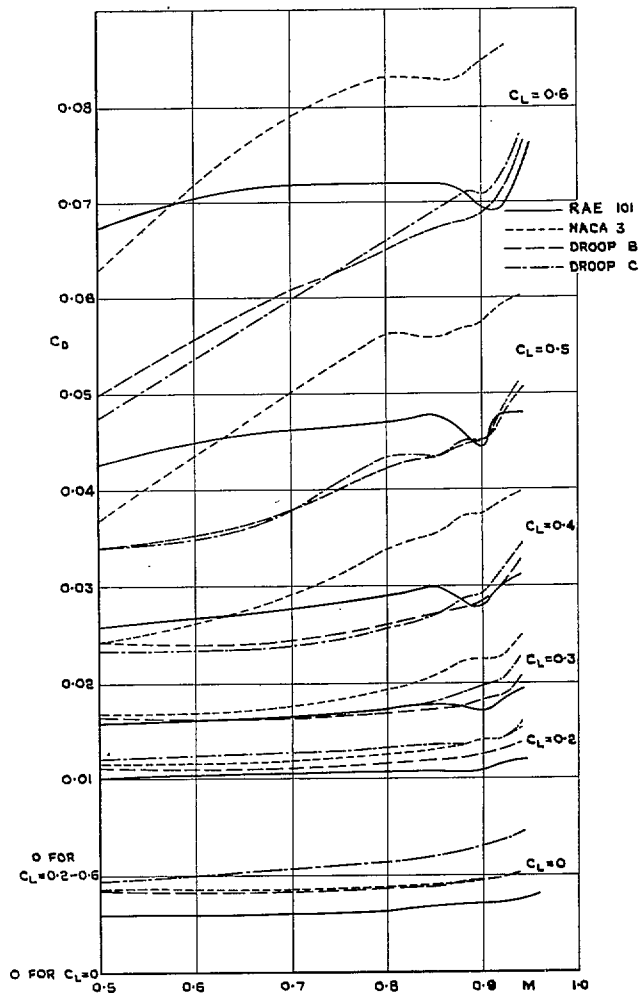

FIG. 13. C_D vs. Mach number at various lift coefficients. Effect of section shape. $R \sim 1{\cdot}7 \times 10^6$ (Section 4.5).

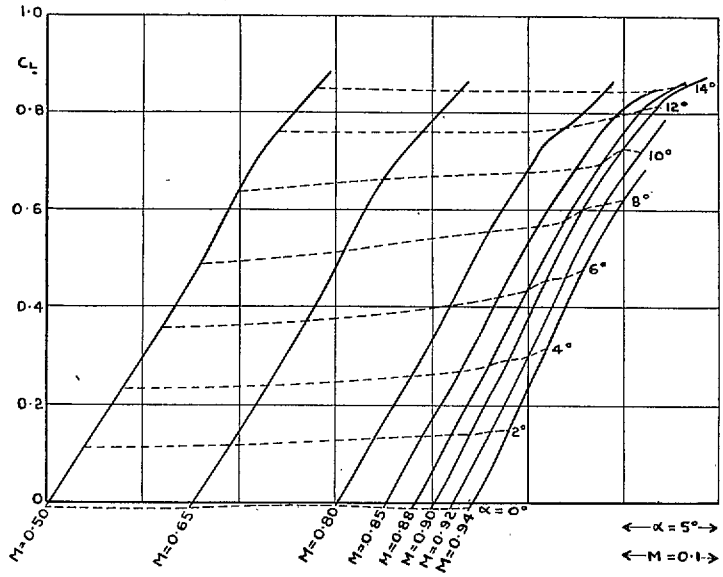

FIG. 14a. Lift carpet, RAE 101 wing, $R \sim 1{\cdot}7 \times 10^6$ (Section 4.1).

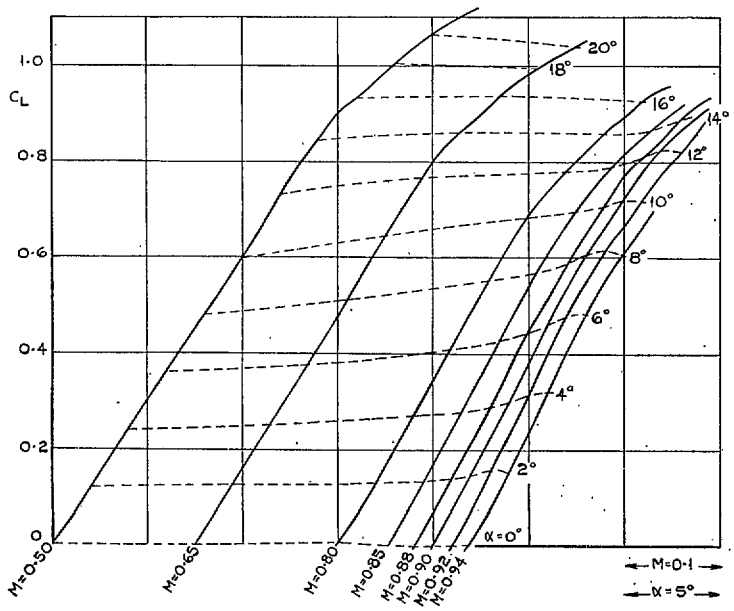

FIG. 14b. Lift carpet, wing B, $R \sim 1{\cdot}7 \times 10^6$ (Section 4.1).

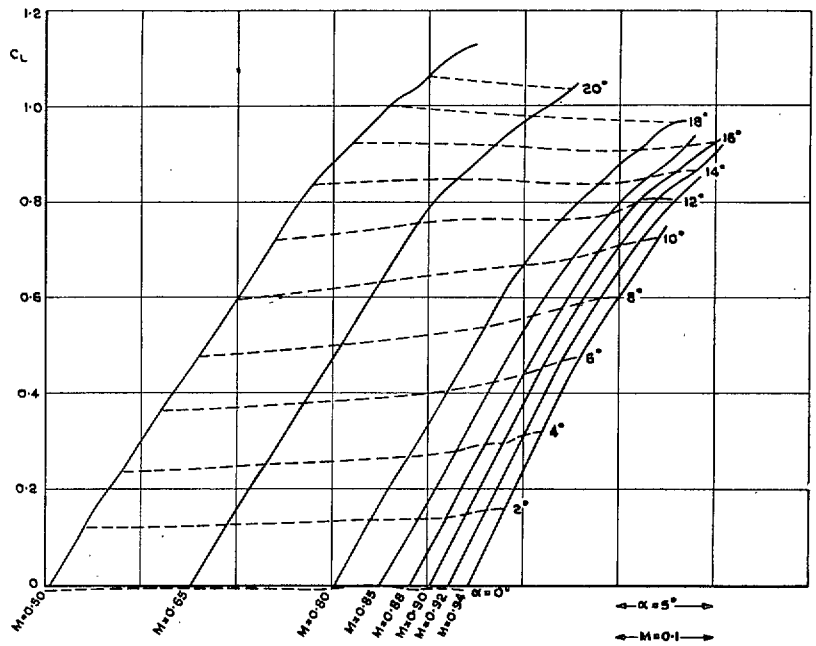

FIG. 14c. Lift carpet, wing C, $R \sim 1{\cdot}7 \times 10^6$ (Section 4.1).

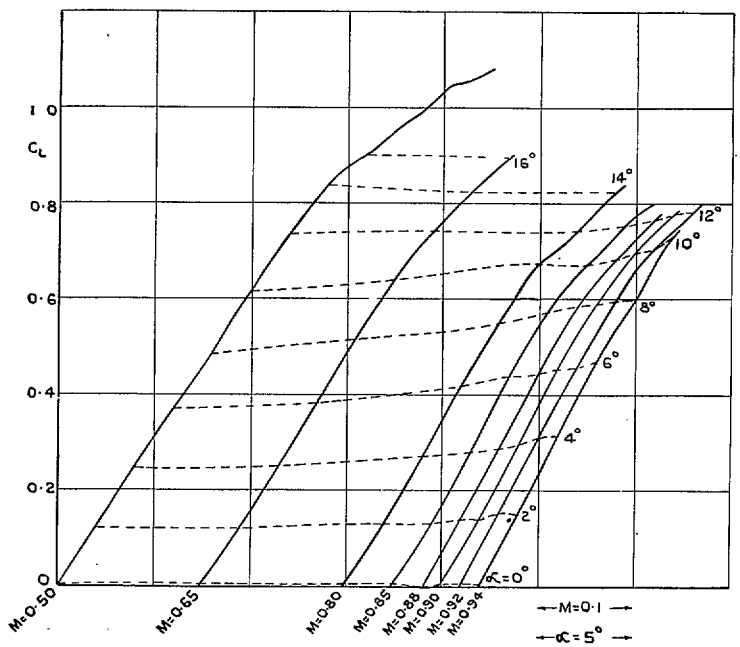

FIG. 14d. Lift carpet, NACA 3 wing, $R \sim 1{\cdot}7 \times 10^6$ (Section 4.1).

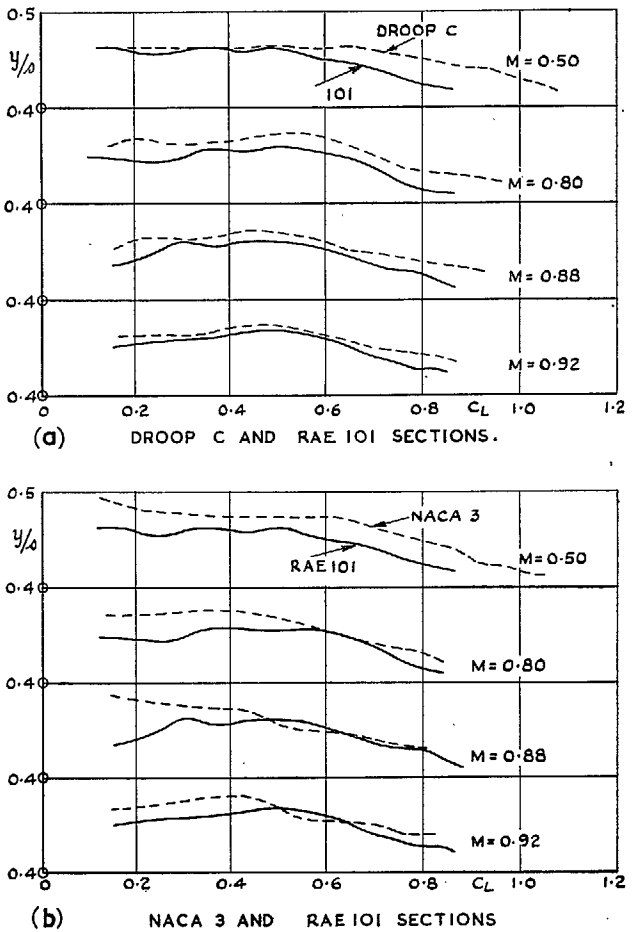

FIG. 15a and b. Spanwise centre of load vs. C_L at various Mach numbers. $R \sim 1{\cdot}7 \times 10^6$ (Sections 4.2, 4.4).

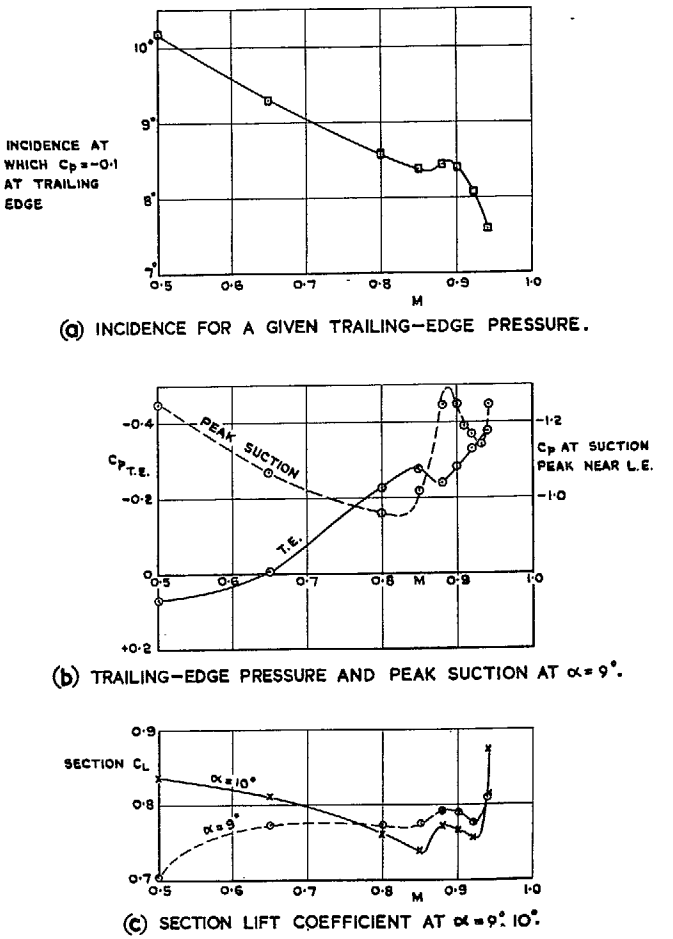

FIG. 16a to c. Effect of Mach number on trailing-edge pressure, peak suction and local C_L at $0{\cdot}72 \times$ semi-span. RAE 101 wing, $R \sim 1{\cdot}7 \times 10^6$ (Section 4.1).

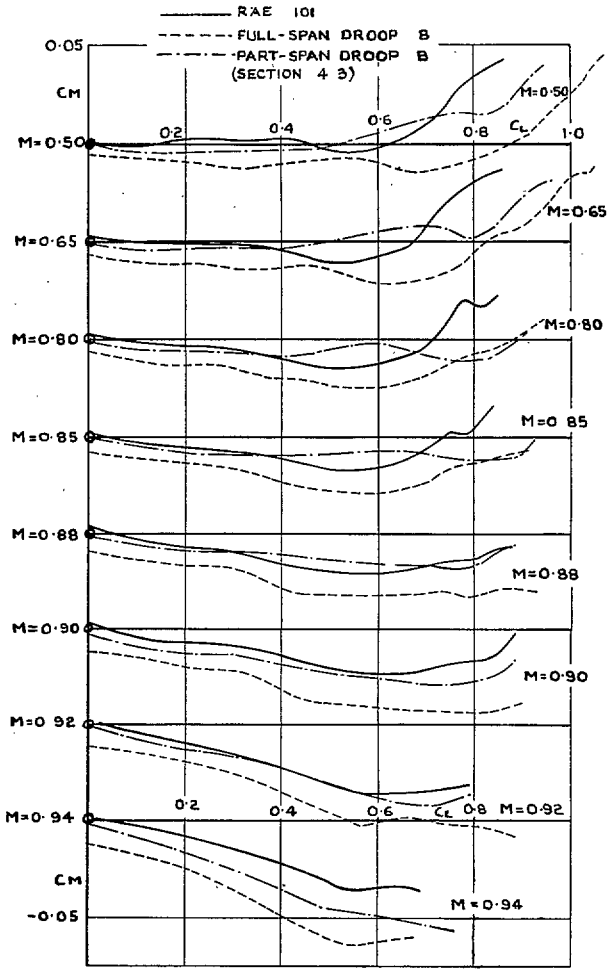

FIG. 17. C_M vs. C_L for full-span and part-span droop B at various Mach numbers. $R \sim 1{\cdot}7 \times 10^6$ (Section 4.3).

(82537) Wt. 66/991 K.5 10/61 Hw.

Publications of the Aeronautical Research Council

ANNUAL TECHNICAL REPORTS OF THE AERONAUTICAL RESEARCH COUNCIL (BOUND VOLUMES)

1941 Aero and Hydrodynamics, Aerofoils, Airscrews, Engines, Flutter, Stability and Control, Structures. 63*s.* (post 2*s.* 3*d.*)

1942 Vol. I. Aero and Hydrodynamics, Aerofoils, Airscrews, Engines. 75*s.* (post 2*s.* 3*d.*)
Vol. II. Noise, Parachutes, Stability and Control, Structures, Vibration, Wind Tunnels. 47*s.* 6*d.* (post 1*s.* 9*d.*)

1943 Vol. I. Aerodynamics, Aerofoils, Airscrews. 80*s.* (post 2*s.*)
Vol. II. Engines, Flutter, Materials, Parachutes, Performance, Stability and Control, Structures. 90*s.* (post 2*s.* 3*d.*)

1944 Vol. I. Aero and Hydrodynamics, Aerofoils, Aircraft, Airscrews, Controls. 84*s.* (post 2*s.* 6*d.*)
Vol. II. Flutter and Vibration, Materials, Miscellaneous, Navigation, Parachutes, Performance, Plates and Panels, Stability, Structures, Test Equipment, Wind Tunnels. 84*s.* (post 2*s.* 6*d.*)

1945 Vol. I. Aero and Hydrodynamics, Aerofoils. 130*s.* (post 3*s.*)
Vol. II. Aircraft, Airscrews, Controls. 130*s.* (post 3*s.*)
Vol. III. Flutter and Vibration, Instruments, Miscellaneous, Parachutes, Plates and Panels, Propulsion. 130*s.* (post 2*s.* 9*d.*)
Vol. IV. Stability, Structures, Wind Tunnels, Wind Tunnel Technique. 130*s.* (post 2*s.* 9*d.*)

1946 Vol. I. Accidents, Aerodynamics, Aerofoils and Hydrofoils. 168*s.* (post 3*s.* 3*d.*)
Vol. II. Airscrews, Cabin Cooling, Chemical Hazards, Controls, Flames, Flutter, Helicopters, Instruments and Instrumentation, Interference, Jets, Miscellaneous, Parachutes. 168*s.* (post 2*s.* 9*d.*)
Vol. III. Performance, Propulsion, Seaplanes, Stability, Structures, Wind Tunnels. 168*s.* (post 3*s.*)

1947 Vol. I. Aerodynamics, Aerofoils, Aircraft. 168*s.* (post 3*s.* 3*d.*)
Vol. II. Airscrews and Rotors, Controls, Flutter, Materials, Miscellaneous, Parachutes, Propulsion, Seaplanes, Stability, Structures, Take-off and Landing. 168*s.* (post 3*s.* 3*d.*)

Special Volumes

Vol. I. Aero and Hydrodynamics, Aerofoils, Controls, Flutter, Kites, Parachutes, Performance, Propulsion, Stability. 126*s.* (post 2*s.* 6*d.*)
Vol. II. Aero and Hydrodynamics, Aerofoils, Airscrews, Controls, Flutter, Materials, Miscellaneous, Parachutes, Propulsion, Stability, Structures. 147*s.* (post 2*s.* 6*d.*)
Vol. III. Aero and Hydrodynamics, Aerofoils, Airscrews, Controls, Flutter, Kites, Miscellaneous, Parachutes, Propulsion, Seaplanes, Stability, Structures, Test Equipment. 189*s.* (post 3*s.* 3*d.*)

Reviews of the Aeronautical Research Council

1939–48 3*s.* (post 5*d.*) 1949–54 5*s.* (post 5*d.*)

Index to all Reports and Memoranda published in the Annual Technical Reports

1909–1947 R. & M. 2600 6*s.* (post 2*d.*)

Indexes to the Reports and Memoranda of the Aeronautical Research Council

Between Nos. 2351–2449	R. & M. No. 2450 2*s.* (post 2*d.*)
Between Nos. 2451–2549	R. & M. No. 2550 2*s.* 6*d.* (post 2*d.*)
Between Nos. 2551–2649	R. & M. No. 2650 2*s.* 6*d.* (post 2*d.*)
Between Nos. 2651–2749	R. & M. No. 2750 2*s.* 6*d.* (post 2*d.*)
Between Nos. 2751–2849	R. & M. No. 2850 2*s.* 6*d.* (post 2*d.*)
Between Nos. 2851–2949	R. & M. No. 2950 3*s.* (post 2*d.*)
Between Nos. 2951–3049	R. & M. No. 3050 3*s.* 6*d.* (post 2*d.*)

HER MAJESTY'S STATIONERY OFFICE

from the addresses overleaf

Printed and published by
Her Majesty's Stationery Office

To be purchased from
York House, Kingsway, London w.c.2
423 Oxford Street, London w.1
13a Castle Street, Edinburgh 2
109 St. Mary Street, Cardiff
39 King Street, Manchester 2
50 Fairfax Street, Bristol 1
2 Edmund Street, Birmingham 3
80 Chichester Street, Belfast 1
or through any bookseller

Printed in England

S.O. Code No. 23–3230